БИОМЕДИЦИНСКА ТЕХНИКА
/
BIOMEDICAL ENGINEERING

(БТ/BTI)

EMG feedback for improved control of myoelectric hand prostheses

Strahinja Dosen, Pranav Mamidanna, Jack Tchimino, Filip Gasparic, Nikola Jorgovanovic

***Abstract*—Myoelectric prostheses can compensate for the motor functions that are lost due to an amputation. However, none of the commercial prostheses restores somatosensory feedback to their users. A conventional approach to providing the missing sensory information is to read the data from the sensors embedded in the prosthesis and transmit this information back to the subject by stimulating the skin of the residual limb mechanically or electrically. However, we have proposed a substantially different approach to closing the control loop. In this scheme, the tactile feedback does not convey the output of the prosthesis (sensor data) but its command input, namely, the magnitude of the myoelectric signals generated by the user (so-called EMG feedback). In this lecture, we will explain that this method facilitates the natural proprioceptive feedback from the muscles (sense of contraction) and thereby allows predictive control of prosthesis grasping force. We will also present results illustrating that EMG feedback outperforms conventional force feedback in terms of accuracy and robustness. Finally, we will outline the potential for further developments of this approach.**

***Index Terms*—myoelectric prostheses, tactile feedback, electrotactile and vibrotactile stimulation, EMG feedback, grasping force control.**

I. Conventional approach to closing the loop

To fully reconstruct the limb that is lost due to an amputation, a bionic prosthesis should restore both motor and sensory functions. Myoelectric control allows an intuitive connection between the brain of the user and his/her prosthesis; however, commercial devices do not transmit somatosensory feedback. Therefore, the amputees do not "feel" their bionic limbs, which might impair performance during prosthesis use as well as the sense of embodiment.

Modern hand prostheses are equipped with sensors and the feedback can be restored by translating sensor data into stimulation profiles that are delivered to the residual limb using mechanical or electrical stimulation [1]. For instance, the magnitude of the grasping force can be associated with the frequency or intensity of electrical stimulation applied to the surface of the skin. The prosthesis user can then learn to interpret the elicited sensations – faster or stronger stimulation indicates larger forces.

Recognizing the importance of sensory feedback in able-bodied subjects, the expectation was that providing such artificial force feedback to an amputee user would significantly improve the performance. The results in the literature are however contradictory [2]. Some studies indeed show an improvement, while in some, the addition of feedback was not beneficial.

Strahinja Došen, Pranav Mamidanna, and Jack Tchimino are with the Department of Health Science and Technology, Aalborg University, Frederik Bajers Vej 7D 9220, Aalborg, Denmark ({sdosen, prma, itc}@hst.aau.dk).

Filip Gašparić and Nikola Jorgovanovic are with the Faculty of Technical Sciences, University of Novi Sad, 6 Trg Dositeja Obradovića, 21000 Novi Sad, Serbia (e-mail: {filip.gasparic, nikolaj}@uns.ac.rs).

II. EMG feedback: an approach inspired by human motor control

In this lecture, we will first explain that the controversial results in literature can be understood by approaching the topic of artificial sensory feedback from the perspective of human motor control [2]. We will then use the same framework to introduce a different approach to closing the loop, so-called EMG feedback [3]. In this method, the tactile stimulation is not used to convey sensor data (prosthesis output); instead, it transmits the magnitude of the myoelectric signal generated by the user as the command input for the prosthesis. Since the prosthesis responds proportionally to the input signal, EMG feedback enables the subject to control the grasping force predictively.

The usual approach for the implementation of EMG feedback is to divide the myoelectric signal into ranges, where each range is indicated by a simple stimulation pattern, e.g., activation of a specific vibration motor from an array of motors placed around the residual limb [4], [5]. To produce a specific force level, the subject then needs to activate his/her muscles and increase the muscle contraction until he/she feels that the desired motor is on. Then, the subject maintains that contraction level, while the prosthesis closes and produces the desired force. Contrary to the conventional approach, the feedback is in this case available even before the prosthesis makes contact with an object, giving enough time for adjustments.

We will present the results from our recent experiments illustrating this approach and showing that EMG feedback outperforms the conventional method in terms of both accuracy and robustness. We will then present the ideas for the further developments of EMG feedback.

References

[1] S. J. Bensmaia, D. J. Tyler, and S. Micera, "Restoration of sensory information via bionic hands," *Nat. Biomed. Eng.*, Nov. 2020.

[2] J. W. Sensinger and S. Dosen, "A Review of Sensory Feedback in Upper-Limb Prostheses from the Perspective of Human Motor Control," *Front. Neurosci.*, vol. 14, Jun. 2020.

[3] S. Dosen, M. Markovic, K. Somer, B. Graimann, and D. Farina, "EMG Biofeedback for online predictive control of grasping force in a myoelectric prosthesis.," *J. Neuroeng. Rehabil.*, vol. 12, no. 1, p. 55, Jun. 2015.

[4] M. A. Schweisfurth, M. Markovic, S. Dosen, F. Teich, B. Graimann, and D. Farina, "Electrotactile EMG feedback improves the control of prosthesis grasping force," *J. Neural Eng.*, vol. 13, no. 5, p. 056010, Oct. 2016.

[5] J. Tchimino, M. Markovic, J. L. Dideriksen, and S. Dosen, "The effect of calibration parameters on the control of a myoelectric hand prosthesis using EMG feedback," *J. Neural Eng.*, vol. 18, no. 4, p. 046091, Aug. 2021.

Wireless Sensing and Control of Actuation for Machines and Humans

Nenad Jovičić

***Abstract*—To a greater or lesser extent, wireless sensors and control systems have been used for decades in various areas of life and work. First implementations in the industry were intended for reliable transmission of simple remote control commands. Manipulating machines without complicated wiring has encouraged the creation of many ideas for applying wireless technologies in biomedical engineering. However, biomedical systems were often unpredictable, the operation in the environment in which they were applied was not always controllable, and as it turned out that simple technology transfer between industry and human applications was not trivial, sometime even inappropriate.**

Expansion of consumer market and development of computer networks and mobile telephony in the last decades led to the rapid growth of many wireless standards resulting in broadband, narrowband, personal, local, global, and other wireless technologies. The development of technology gives a new impetus to its applications in industry and afterward in life sciences and medicine.

The talk is a retrospective of historical, past, present, and future challenges faced by wireless systems used in industry and biomedicine. Typical industrial and biomedical applications will be analyzed where different parameters like high bandwidth, low latency, or high energy efficiency are essential. Insights on how new wireless standards enable us to apply modern methods of big data processing, cloud computing, and artificial intelligence will be given. The special attention will be put on the bottlenecks in domains of security and reliability.

Finally, the theoretical analysis will be supported by two examples of use of Wi-Fi wireless communication, on one industrial and one biomedical system.

***Index Terms*—wearable system, wireless communication, industry, biomedicine, standards, security, reliability**

Nenad Jovičič is Associate professor of Electronics, School of Electrical Engineering, University of Belgrade., Bulevar kralja Aleksandra, 11020 Belgrade, Serbia (e-mail: nenad@etf.bg.ac.rs).

A Measure of Spasticity Based on the Exponential Fit of the Knee Joint Torque Estimated from the Goniogram During the Pendulum Test

Antonina Aleksić, Dejan B. Popović, *Member, IEEE*

***Abstract*— Pendulum test is a method to quantify the spasticity. We used the goniogram recorded during the pendulum test to estimate the knee joint torque based on the model which considers spastic reflex activity. We fitted the exponential curve $T_h = ae^{-bt}$ to the estimated knee joint torque to calculate the parameters a and b. We compared the scaled value log a/b with the modified Ashworth score. We used 8 sets of data collected in a clinical study with six complete paraplegic subjects. The comparison shows that the ratio a/b correlates with the MAS scores; thereby, can be used as a measure of spasticity. The advantage of using the ratio a/b is that this score is not rater dependent and that the scores are real numbers compared the MAS scores; thereby, providing better resolution of the level of spasticity.**

***Index Terms*—spinal cord injury; pendulum test; spasticity; modelling**

I. Introduction

Spasticity often follows nervous system lesions at the cortical and spinal levels (e.g., spinal cord injury, multiple sclerosis, cerebral palsy). The spasticity is defined as a motor disorder characterized by a velocity-dependent increase in tonic stretch reflexes ("muscle tone") with exaggerated tendon jerk, resulting from hyperexcitability of the stretch reflex, as one of the components of the upper motor neuron syndrome [1]. For clinicians, the quantification of the spasticity is of interest to select the most appropriate therapy for the patient. The modified Ashworth Scale (MAS) is the most often method to score the spasticity [2]. The MAS based assessment is characterized by interrater and intrarater reliability [3-5]. Therefore, Wartenberg introduced the pendulum test to eliminate the subjective component when assessing spasticity [6]. The model was expanded by Bajd and Vodovnik [7], Bajd and Bowman [8], and mc later Le Cavorzin et al. [9-11].

Our group recently introduced a score termed Pendulum Test (PT) score [12]. The clinical study proved that the PT score is correlated with MAS [12]. In addition, we used the complex biomechanical model of the pendulum type lower leg movements, and introduced the new measure termed SPASticity Scale (SPAS) [14]. Here we present the correlation of SPAS and MAS on data from 48 pendulum tests and show that the SPAS is more sensitive compared with MAS and show the type of spasticity; thereby, that is useful for clinicians.

.

Antonina Aleksić is with Institute of Technical Sciences of the Serbian Academy of Sciences and Arts, Knez Mihailova 35/IV, Belgrade, Serbia.(e-mail: aleksicantonina@gmail.com)

Dejan B. Popović is with Serbian Academy of Sciences and Arts, Knez Mihailova 35, Belgrade, Serbia and Aalborg University, Aalborg, Denmark (e-mail: dbp@ etf.rs).

II. The Method

A. Subjects

The data were recorded within the clinical study reported in [14]. Six subjects signed the consent approved by the Clinic for rehabilitation "Dr Miroslav Zotović", Belgrade, Serbia. The inclusion criteria were: 1) a complete lesion above the Th12; 2) a stable neurological and medical status; 3) no autonomic dysreflexia; 4) no cognitive disorders; and 5) no medical history of hearing or balance disorders. The recordings were done four times during two sessions. This provided 48 data sets for the analysis.

B. Instrumentation

The pendulum test was recorded using a device that consists two units: one unit mounted at the thigh comprising an amplifier for two electromyography (EMG) signals and an inertial measurement unit - IMU (3D accelerometer and 3D gyroscope), and the second IMU mounted at the shank (Fig. 1, left panel). The sampling frequency of the EMG signal was 1kHz. Both units sent a signal to the host computer wirelessly at 1000 samples per second. More about the device can be found in [15].

C. Data processing

All the data processing was done using MATLAB (Mathworks, Natick, USA). The motion can be modeled with the nonlinear model which includes the passive resistance and the active resistance due to involuntary activity of the stretched paralyzed muscles during the pendulum like movements of the lower leg about the immobile knee. The equation of the motion is the following:

$$J\ddot{\varphi} = -B\dot{\varphi} - K\varphi - \frac{1}{2}mgl\sin\varphi + T_h \quad (1)$$

φ is the knee joint angle measured to the gravity line, *J* is the moment of inertia for the lower leg, *B* and *K* are the damping and stiffness coefficients of the linear model of passive resistance at the knee joint, *m* is the mass of the shank/foot complex, *l* the length from the knee to sole. The torque *Th*

represents involuntary activities of the paralyzed knee extensors and flexors

$$T_h = T_E(\varphi, \dot{\varphi}) - T_F(\varphi, \dot{\varphi}) \qquad (2)$$

We fitted the recorded goniogram φ *(t)* with the minimum quadratic error method with the model (1) and (2) and calculated the knee joint torque *Th*. The next step was the fit the exponential curve to the calculated torque.

$$T_h = ae^{-bt} \qquad (3)$$

The output from the fitting were the numbers *a* and *b*. We than defined the measure SPAS to limit that output to the range of the scorers of the MAS.

$$SPAS=4 * \log|a/b| \qquad (4)$$

More detail can be found in Aleksić [14].

D. Procedure

The subject was sitting on a stable desk with the stable back support, with the hip angle $\varphi \approx 135°$. The thigh was resting on a flat surface while the knee was in front of the edge of the table to allow free rotation of the lower leg about the joint. The pendulum test was performed on each subject 4 times in 2 recording sessions. The examiner extended the knee joint to the full extension ($\varphi \approx \pi/2$), released it, and the lower leg started damped oscillations which stopped in vertical position ($\varphi \approx 0$).

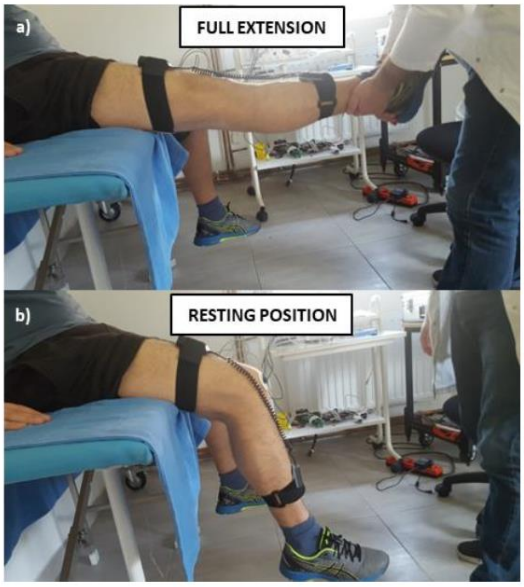

Fig. 1. The setup showing the initial and terminal position of the lower leg during the pendulum test (modified from [15]).

III. Main Results

Figure 1 shows the scaled goniogram of the knee joint by the dashed black line, the calculated moment *Th* shown in red, and the exponential fit in blue. The top two traces show spastic EMG signals that are directly related to the spasticity and the reason of disrupting the normal pendulum like movement in the field of gravity.

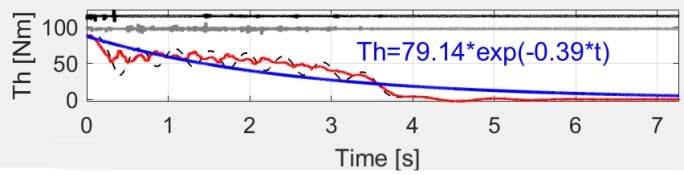

Fig. 2. An example of the estimated torque and the exponential fit for one of the subjects. Red line shows the estimated torque *Th*, the blue line and the equation represent the best exponential fit to the torque *Th*. The dashed black line shows the scaled goniogram of the knee joint $\varphi(t)$ that starts from $\pi/2$ and ends at 0. The black and grey traces at the top are the measured EMG signal (< ±0,5mV) of the knee joint flexors and extensors, respectively.

The MAS and the SPAS values for all the subjects that participated in the study are in Table I.

TABLE I
MAS AND SPAS SCORES FOR THE SIX SUBJECTS ESTIMATED FOUR TIMES IN EACH OF THE TWO RECORDINGS SESSIONS (F - FIRST RECORDING SESSION, S - SECOND RECORDING SESSION)

Nº	1st MAS	1st SPAS	2nd MAS	2nd SPAS	3rd MAS	3rd SPAS	4th MAS	4th SPAS
1f	3	2.43	3	2.24	3	3.24	3	1.30
1s	3	2.97	3	1.52	3	2.89	3	2.31
2f	2	2.62	1	0.67	1	2.02	2	1.63
2s	2	1.83	1	1.90	1	2.01	1	1.55
3f	1	1.19	1	0.78	1	1.22	1	1.50
3s	2	4.80	4	4.85	2	5.13	2	3.66
4f	2	1.75	2	0.78	2	0.74	2	0.98
4s	2	1.16	2	0.08	2	0.41	1	0.32
5f	3	5.68	3	5.52	3	4.76	3	4.88
5s	3	3.78	2	2.21	2	2.94	2	2.35
6f	2	0.63	2	1.00	2	0.34	1	0.08
6s	2	0.31	1	0.17	1	0.17	1	0.17

Data from Table I is presented in Fig. 3. We applied the linear regression and obtained that SPAS = 1.06 MAS -0.12, R^2=0.31 when plotting SPAS vs. MAS.

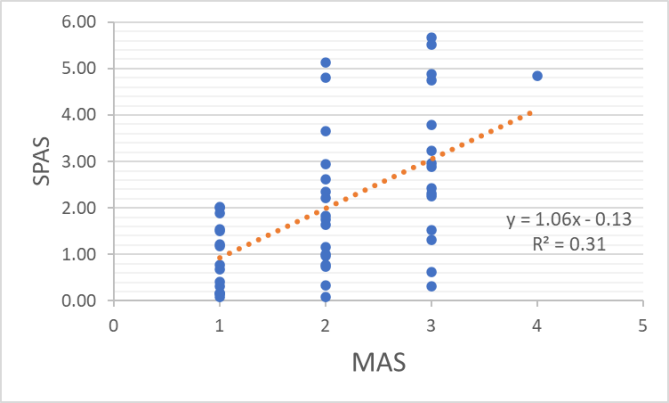

Fig. 3. The SPAS vs. MAS scores and the linear regression for all 48 recording sessions

Figure 4 shows the linear regression of the SPAS vs. MAS without the outliers. The outliers were chosen as the two greatest and lowest SPAS measures for MAS scores 1, 2 and 3. This outlier elimination left for the analysis 36 recordings. The linear regression was SPAS = 0.94 MAS – 0.15, R^2=0.55.

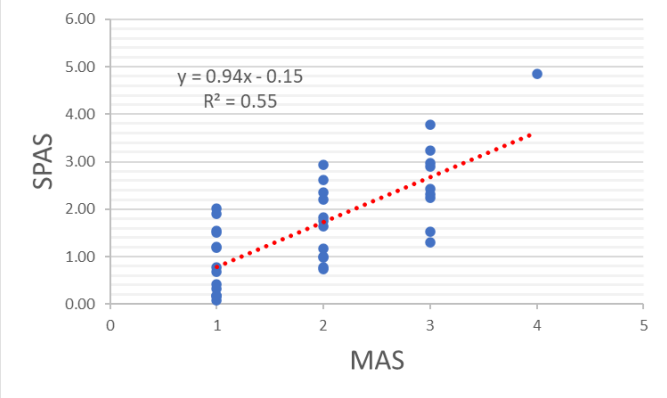

Fig. 4: The linear regression of SPAS vs. MAS of data from 36 recordings.

Figure 5 shows the SPAS and MAS scores from eight recordings for Subject 1 (1f and 1s).

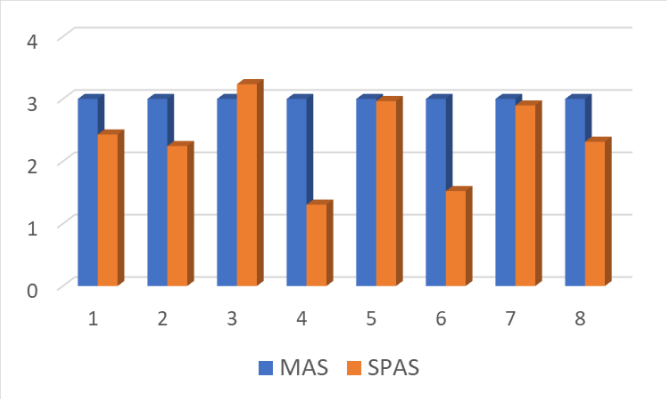

Fig. 5: Bar graph showing the MAS and SPAS scores for Subject 1 (1f and 1s) in eight recordings.

IV. Discussion

Table 1, gives an insight into SPAS and MAS comparison. The graphical presentation of this data (Fig. 3) with the linear fit to has the slope of y=1.06, and R2=0.3. When we exclude 12 outliers, the linear fit equation is y= 0.94x - 0.15, yet with the increased value R^2=0.55. The slope is now smaller compared to the slope with all data, but also close to 1.

In Fig. 5 we show the comparison of the MAS and SPAS for Subject 1. Here, the MAS grade was constant and equal to 3. The SPAS grade varied, being smallest for the fourth recording SPAS=1.3, and highest for the fifth recordings, SPAS=2.97. This clearly suggests how much is the SPAS more sensitive compared with the MAS.

V. Conclusion

We show the relation between the MAS and SPAS scores. Due to the fact that MAS is an integer value and the SPAS is a real number, the sensitivity of the SPAS scale is better compared with the MAS. This increased sensitivity is important for the clinician when deciding which therapy works and following the progress of the recovery of the patient. The SPAS is a measure that automatically determined from the goniogram of the knee joint during the pendulum test.

Acknowledgment

This research was supported by the Ministry of education, science and technology of Republic of Serbia, by the Contract of financing scientific work of Institute of Technical Sciences of the SASA (451-03-9/2021-14/200175) and partly by the Serbian Academy of Sciences and Arts.

We thank PhD Lana Popović Maneski for the support with the instrumentation for the pendulum test and sggestions for the interpretation of data. We thank Radoje Čobeljić, M.D, Ph.D. from the Clinic of rehabilitation “Dr. Miroslav Zotović”, Belgrade for the instrumental works with patients and the MAS scoring.

References

[1] [1] J. W. Lance, ”Pathophysiology of spasticity and clinical experience with baclofen”, In: Lance J. W., Feldman R. G., Young R.R. and Koella W. P. (Eds.), *Spasticity: disordered motor control, Chicago, USA*,pp. 185-203, 1980, Year Book Medical Publishers,

[2] [2] R. W. Bohannon, M. B. Smith, “Interrater reliability of a modified Ashworth scale of muscle spasticity ”*Phys ther*, pp. 206-207, vol. 67, no. 2, Feb, 1987.

[3] [3] C. Trompetto, L. Marinelli, L. Mori, E. Pelosin, A. Currà, L. Molfetta, G. Abbruzzese. Pathophysiology of spasticity: implications for neurorehabilitation. *BioMed research international* 2014,

[4] [4] M. Blackburn, P. Van Vliet, S.P. Mockett, “Reliability of measurements obtained with the modified Ashworth scale in the lower extremities of people with stroke”,*Physical therapy* vol. 82 no. 1, pp. 25-34, 2002.

[5] [5] A. D. Pandyan, G.R. Johnson, C. I.Price CI, R. H. Curless, M.P. Barnes, H. Rodgers, “A review of the properties and limitations of the Ashworth and modified Ashworth Scales as measures of spasticity”,*Clinical rehabilitation*, vol. 13, no. 5, pp. 373-383, 1999.

[6] [6] R. Wartenberg, “Pendulousness of the legs as a diagnostic test.” Neurology, vol. 1, pp, 18-24, 1951.

[7] [7] T. Bajd, L.Vodovnik. “Pendulum testing of spasticity.” Journal of Biomedical Engineering., vol. 6, no 1. , pp. 9-16, Jan. ,1984

[8] [8] Bajd T, Bowman B. Testing and modelling of spasticity. *Journal of biomedical engineering* vol. 4. no. 2, pp.90-96, 1982.

[9] [9] P. Le Cavorzin, X. Hernot, O. Bartier,H. Allain, G. Carrault,P. Rochcongar, F.Chagneau, “ A computed model of the pendulum test of the leg for routine assessment of spasticity in man” , *ITBM-RBM* vol. 22 no. 3, pp. 170-177, 2001.

[10] [10] P. Le Cavorzin, S.A. Poudens, F. Chagneau, G. Carrault, H. Allain, P. Rochcongar P. “A comprehensive model of spastic hypertonia derived from the pendulum test of the leg”. *Muscle & nerve*, vol. 24 no.12, pp.1612-1621,2001.

[11] [11] P.Le Cavorzin, G. Carrault, F. Chagneau, P. Rochcongar, ,H. Allain. A computer model of rigidity and related motor dysfunction in Parkinson's disease. *Movement disorders: official journal of the Movement Disorder Society* 2003; vol. 18, no.11, pp. 1257-1265.

[12] [12] L. Popović-Maneski, A. Aleksić, A. Metani, V. Bergeron, R. Čobeljić and D. B. Popović, “Assessment of Spasticity by a Pendulum Test in SCI Patients Who Exercise FES Cycling or Receive Only Conventional Therapy.” IEEE Trans Neural Syst Rehabil Eng,, vol. 26, no. 1, pp. 181-187, Jan., 2018.

[13] [13] L. Popović-Maneski, A. Aleksić, R. Čobeljić, T. Bajd, D. B. Popović. “A new method and trumentation for analyzing spasticity.” IETI Trans on Ergonomics and Safety, vol. 1, no. 1, pp. 12-27, Jan., 2017.

[14] [14] A. Aleksić, D.B.Popović, **"**New scale for assessing spasticity based on the pendulum test", Computer Methods in Biomechanics and Biomedical Engineering. in review
[15] [15] M. Miletić, V. Atanasoski, J. Kršić, A. Lazović, and L. Popović-Maneski, "Validation of the new wearable instrument for the pendulum test based on inertial sensors", IcETRAN 2020, 7th International Conference on Electrical, Electronic and Computing Engineering, Belgrade, Serbia, September, 2020.

Multiple measurements by a pendulum test improve the spasticity assessment in SCI subjects

Nikola Babić, Radoje Čobeljić, Slađana Kostić-Smith, Lana Popović-Maneski

***Abstract*— We present the variability of the spasticity scores during three consecutive days using the case series clinical study data with spinal cord injured (SCI) subjects. We assessed the spasticity by the Pendulum Test (PT) and Ashworth Scale (AS) scores. We measured the spasticity on the three consecutive days before and after the period of the treatment. Three subjects with SCI participated in the study. We found large variability from day to day. The PT score had more significant variability compared with the AS. The results suggest that the three consecutive testing by using the pendulum test and PT score on different days provide a better assessment of spasticity being essential in evaluating the treatment protocol.**

***Index Terms*— Spasticity assessment; Pendulum test; PT score; Ashworth Scale; Spinal cord injury.**

I. Introduction

UPPER motor neuron lesions lead to hypertonia resulting in paralysis/paresis of extremities [1]. Spasticity caused by a spinal cord injury (SCI) affects the quality of life of subjects with paralysis. Since neurological recovery is a long process, precise information on spasticity changes could assist in selecting the optimal treatment procedures. A research study that included 110 subjects after SCI shows a significant role in the severity of spasticity of the quality of life when using the Quality of life scores [2].

The validated, most often used methods for assessing the severity of spasticity use the Ashworth scale (AS) and modified Ashworth scale (MAS). AS and MAS score the reaction of manipulating the segment of the body that stretches the muscles responsible for the flexion and extension of the specific joint analyzed. The reaction is assessed physically by the examiner. The fact that the score reflects the examiners' perception of paralyzed muscles' involuntary response makes it inter-rater dependent; therefore, subjective.

The pendulum test (PT) was introduced to get an objective measure of the severity of spasticity. In the PT, the examiner stretches the muscles to bring the body segment into the position where gravity will cause the pendulum-like movement when the examiner lets the body segment free. The PT is convenient for the knee and elbow joints. The PT was used in the severity of spasticity scoring in subjects with spinal cord injuries [3, 4]; cerebral palsy [5, 6]; cerebrovascular insults [3, 7]; and sclerosis multiplex [8].

The PT increases the precision, objectivity, reliability, and validity of the spasticity measures [8]. The essential fact is that spasticity varies; hence, even the quantified PT gives results that change with repetitions and change from one to the next assessment session. We decided to analyze the variability of AS and PT scores by determining those in three consecutive days.

Nikola Babić, Ph.D. student, University of Belgrade, Academy of Applied Studies Belgrade, Cara Dušana 254, 11080, Zemun, Serbia (e-mail: splendz@gmail.com).

Radoje Čobeljić, M.D., Ph.D. Clinic for Rehabilitation "Dr Miroslav Zotović", Sokobanjska 13, 11000, Belgrade, Serbia (e-mail: radoje.cobeljic@gmail.com).

Slađana Kostić-Smith M.D., (e-mail: ksladja@hotmail.com).

Lana Popović Maneski, Ph.D. Institute of Technical Sciences of SASA, Knez Mihailova 35.11000, Belgrade, Serbia (e-mail: lanapm13@gmail.com).

II. Methods and Materials

A. Subjects

The inclusion criteria for entering the study were complete or incomplete SCI above Th12 level (American Spinal Cord Injuries Association (ASIA) A and B), no other trauma or neurological diseases, and the ability to follow the test protocol.

The Ethics Committee of the Clinic for Rehabilitation "Dr. Miroslav Zotović," Belgrade, Serbia, approved a protocol prepared along with the Helsinki declaration. All participants signed the informed consent before entering the study. The basic demography of participants in the study is in Table 1.

TABLE I
BASIC DATA FOR THE SUBJECTS

Subject N^{o}	ASIA	SCI lesion (motor/sensory)
1	A	Th6/Th6
2	B	C6/Th10
3	A	Th8/Th8

B. Instrumentation

We used an instrument that consists of two units fixed at the thigh and shank. Each unit has the inertial measurement unit (IMU) measuring the acceleration and angular rate of the thigh and shank. The unit at the thigh has a two-channel electromyography (EMG) amplifier system connected to surface electrodes over the knee extensors (Quadriceps m.) and knee flexors (Hamstrings m.) (https://www.3-x-f.com/products.html#121) The reference electrode was placed at the bony part in the vicinity of the knee joint.

C. Protocol

The experienced examiner (one of the authors of this paper) assessed both legs' flexion and extension spasticity by applying the Ashworth scale (AS). After the AS assessment, the physiatrist performed the pendulum test, and the computer calculated the PT score.

All tests were done before the intake of medications for the reduction of spasticity.

The subject's position was between the lying and sitting position, with the shanks hanging over the table edge. Hips angles were set to about $3\pi/4$ degrees in all tests. The pelvis and the thighs were fixed with tape to the table. The clinician extended the knee joint to bring the shank to the horizontal position (full knee extension) and let the shank swing about the knee joint caused only by gravity force. The oscillations stopped in less than 15 seconds in all subjects.

IMUs and EMG signals were simultaneously recorded during the pendulum-like movements until the lower leg stopped swinging. The EMG recordings allow the analysis of the timing and strength of spastic reflexive contractions of the paralyzed knee extensors and flexors. The kinematics recordings were used to calculate the PT score [7]. The pendulum measurements were repeated three times at approximately 15-second intervals. The AS and pendulum tests were repeated on three consecutive days.

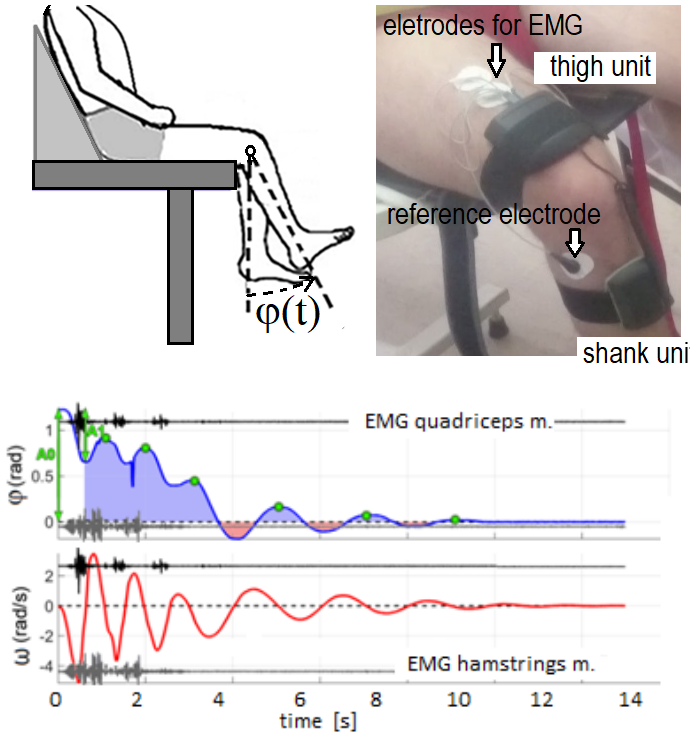

Fig. 1. The setup for the pendulum test with EMG recordings electrodes (upper panel). An example of signals estimated from the recordings: goniogram, tachogram, and the recorded EMG signals (bottom panel).

Fig. 1 shows the knee joint φ(t) and the shank angular rate ω(t) during the pendulum test. The resting position of the shank was vertical (φ = 0). The starting position of the shank in the pendulum test was horizontal (φ = π/2). The blue areas show intervals when the knee joint angle was positive (φ ≥ 0), and the red areas show the intervals when the knee joint was negative (φ < 0). The φ(t) and ω(t) recordings show apparent asymmetry, more precisely, the knee angle is mostly above zero, and there is a significant change in the frequency of oscillations.

EMG signals from the knee extensors (black) and flexors (grey) are shown above and below the goniogram and the tachogram. Fig. 1 shows that the spastic EMG activity stops much before the shank stops oscillating.

The PT score was calculated using the formula defined in Popović Maneski et al. [4]:

$$PT_i = \left|\frac{\left(\bar{R}_{2n_i} - \hat{R}_{2n_H}\right)}{7*\hat{R}_{2n_H}}\right| + \left|\frac{(\bar{N}_i - \hat{N}_H)}{7*\hat{N}_H}\right| + \left|\frac{(\bar{\varphi}_i - \hat{\varphi}_H)}{7*\hat{\varphi}_H}\right| + \left|\frac{\left(\bar{\omega}_{max_i} - \hat{\omega}_{max_H}\right)}{7*\hat{\omega}_{max_H}}\right| + \left|\frac{\left(\bar{\omega}_{min_i} - \hat{\omega}_{min_H}\right)}{7*\hat{\omega}_{min_H}}\right| + \left|\frac{(\bar{f}_i - \hat{f}_H)}{7*\hat{f}_H}\right| + \left|\frac{\left(\left|\frac{\overline{P^+ - P^-}}{P_{total}}\right|_i - \left|\frac{\widehat{P^+ - P^-}}{P_{total}}\right|_H\right)}{7*100}\right| \quad (1)$$

The index H is used for the values of healthy subjects. "i" denotes a subject N°, $\bar{}$ represents a mean value of three trials in the same subject, and ^ represents the mean value for the whole population (i.e., H group population). To normalize PT, each member in the equation is divided by the total number of parameters used to calculate PT (i.e., seven parameters). N is the number of oscillations, $R_{2n} = A_1/1.6A_0$ relaxation index, φ and ω are the knee joint angle and angular rate of the shank, f frequency of oscillations, $P+$ and $P-$ positive and negative area between the knee joint and the neutral value (φ=0), respectively.

III. Results and Discussions

From day to day, we found significant differences in the PT scores. Goniograms with the most significant differences found in the three days of testing are presented (Fig. 2).

Fig. 3 shows the PT and AS scores for three participants in the study for the left and right leg.

The bars indicate that PT scores were different on three subsequent days, while the AS showed more negligible, and in some cases, no variation. We found no rule related to the variability of the PT scores, but this is most likely because the sample of only three subjects is too small. The possible answer will come after a planned randomized clinical study where the statistics are meaningful, and the comparison can be made before and after the treatment.

Figure 4 shows the variability of the results for the measurements on three consecutive days. Although the standard deviation for the left leg in the first and the right in the second day is close to the mean, compared to overall, the data dispersion in the PT scores indicates a higher level of the test sensibility comparing to the AS.

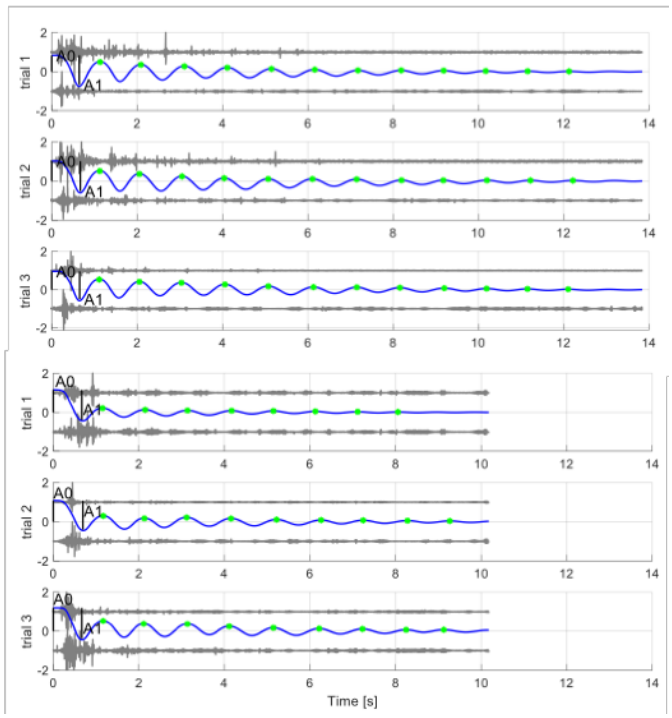

Fig. 2. Goniogram for Subject 1 recorded during the pendulum (right leg). The top three traces are three repetitions during the 1st day, and the bottom three traces are the repetitions on the 2nd day.

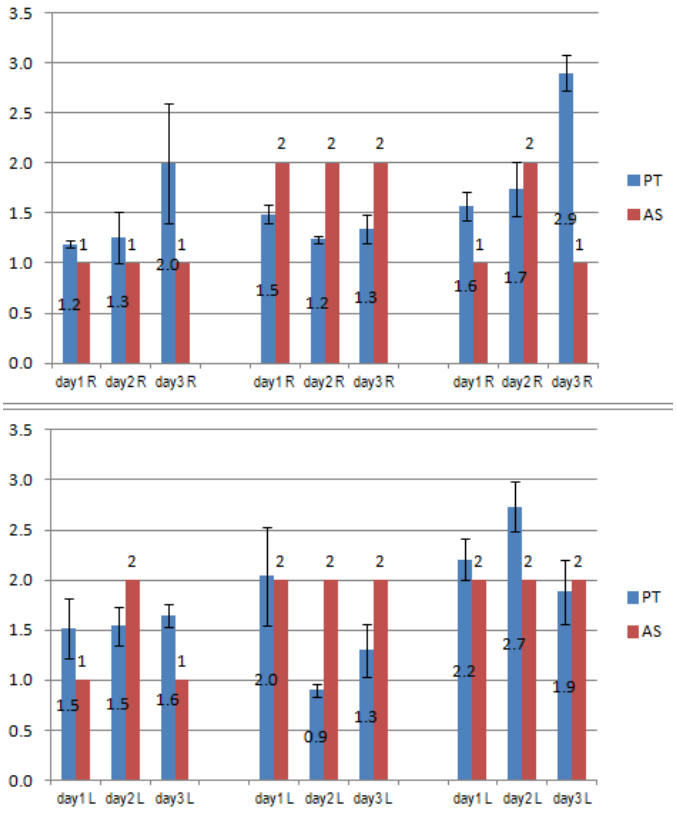

Fig. 3. The PT scores and AS for the right leg (top panel) left and the left leg (bottom panel) for three subjects on three subsequent days.

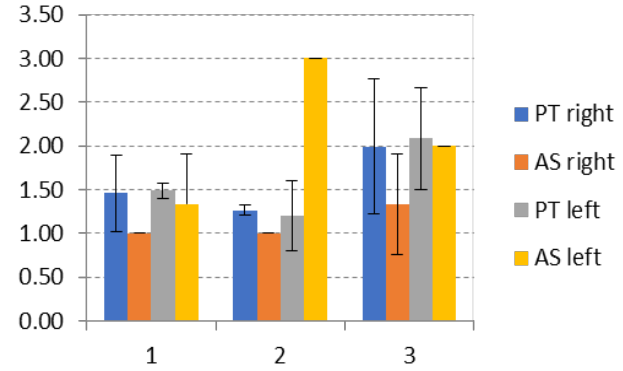

Fig.4. Variability of the PT and AS scores were measured on three consecutive days. The bars show the average score on each day, and the lines are standard deviations.

The size of the study made us present the results by using the means and standard deviations instead of the box-plot presentation.

IV. Conclusion

This case series confirms that precisely detected variability of the spasticity is to be considered in assessing achievements in the rehabilitation progress. Although the variability of the assessment was seen with the Ashworth scale, the precision obtained by the PT score shows that the three consecutive testings on different days are meaningful for the better judgment of spasticity. PT score obtained this way gives precise insight into the spasticity variability, which enables the detection of improvements or deterioration of the subject's condition, thus the nature and extent of effects of a different way of the treatment of spasticity in SCI subjects. The Covid19 pandemic made impossible the inclusion of a more significant number of subjects in the sample and the implementation and evaluation of FES-assisted biking. The findings presented in this paper calls for a more extensive randomized clinical study to be validated.

Acknowledgment

We thank Prof. Dejan B. Popović, from the Serbian Academy of Sciences and Arts (SASA), Belgrade, Serbia, for valuable suggestions and comments related to the final version of the manuscript. We acknowledge the support of physiotherapists Jelena Milovanović and Vladimir Stevanović for performing all the necessary exercises and assistance in measurements. The work on this project was partly supported by the Ministry of Education, Science and Technological Development and contract 451-03-9/2021-14/ 200175 for financing research in ITS-SASA in 2021.

References

[1] C. Trompetto, L. Marinelli, L. Mori, E. Pelosi, A. Currà, L, Molfetta, G. Abbruzzese, "Pathophysiology of spasticity: implications for neurorehabilitation,"Biomed Res Int., 2014.

[2] M. Vural, E.Y. Yalcinkaya, B. Erhan, E.C. Celik, B. Gunduz, A. Bozan, "Assessment of Quality of Life in Relation to Spasticity Severity and

Socio-Demographic and Clinical Factors among Subjects with Spinal Cord Injury, "Journal of Spinal Cord Medicine, vol. 43, no. 2, pp. 193–200, 2020

[3] T, Bajd, L. Vodovnik, "Pendulum testing of spasticity," J Biomed Eng, vol. 6, no. 1, pp. 9-16, Jan 1984.

[4] L. Popović-Maneski, A. Aleksić, A. Metani, V. Bergeron, R. Čobeljić, D.B. Popović. "Assessment of Spasticity by a Pendulum Test in SCI Subjects Who Exercise FES Cycling or Receive Only Conventional Therapy. " IEEE Trans Neural Syst Rehabil Eng." vol. 26, no. 1, pp. 181-187. Jan 2018. DOI: 10.1109/ TNSRE.2017.2771466.

[5] E.G. Fowler, A.I. Nwigwe, T.W. Ho, "Sensitivity of the pendulum test for assessing spasticity in persons with cerebral palsy." Dev Med Child Neurol.; vol. 42, no. 3, pp. 182-189. Mar 2000.

[6] E. Nordmark, G. Anderson. "Wartenberg pendulum test: objective quantification of muscle tone in children with spastic diplegia undergoing selective dorsal rhizotomy." Dev Med Child Neurol. vol. 44. no. 1, pp. 26-33. Jan 2002.

[7] D. B. Popović, T. Bajd. "Pendulum Test: Quantified Assessment of the Type and Level of Spasticity in Persons with Central Nervous System Lesions." Serbian Journal of Electrical Engineering, vol. 15, no. 1), pp. 1–12, Feb 2018.

[8] C.L. Hugos, M.H. Cameron, "Assessment and Measurement of Spasticity in MS: State of the Evidence," Curr Neurol Neurosci Rep, vol 19, no. 79, Aug 2019

[9] P. Decq, P. Filipetti, J.-P. Lefaucheur, "Evaluation of Spasticity in Adults," Operative Techniques in Neurosurgery, Vol 7, no. 3, pp. 100-108, Sep 2004.

Proof of concept platform of an electrotactile Brain Computer Interface

Marija Novičić, Vera Miler-Jerković, Olivera Đorđević, Ljubica Konstantinović and Andrej M. Savić

***Abstract*—The aim of this paper is to present the concept and feasibility test of an electrotactile BCI platform consisted of EEG device, electrical stimulation device of nerves/muscles and custom software platform for device control. The developed application comprised GUI for device settings and synchronization of signal acquisition and stimulation control. Experiments for validation of the platform included trancutaneous electrical stimulation at 2 positions on the forearm for inducing somatosensory evoked potentials in the EEG signals in parallel with the tactile attention task performed by the subject. Initial results show that we were able to successfully acquire SEP with our system and that the tactile attention task modified SEP components in a physiologically congruent manner.**

***Index Terms*—Brain-computer interface; Event-related potentials; Somatosensory evoked potentials; Electrical stimulation.**

I. Introduction

BRAIN-computer interfaces (BCI) allow the direct link between a person's intentions and technical devices without the need for motor control. BCI devices are promising tools in the domain of assistive technologies for people with motor impairments due to neurodegenerative diseases, spinal cord injuries, stroke or brain trauma [1].

BCI control is based on brain signal measurements such as electroencephalography (EEG). Different EEG based control signals can be utilized for driving BCIs, such as event-related potentials, slow cortical potentials or brain oscillatory activity [2]. Those control modalities should enable the user to activate the function based on different mental strategies.

Event-related potentials (ERP) are commonly used BCI control signal and their features have been used for driving BCI based spellers and menus [2]. ERP based BCIs utilize synchronous BCI control where an ERP is elicited by an external stimuli and voluntary control of the device is based on mental strategy of selective attention towards a single stimulus which results in a mismatch in ERP between attended and unattended conditions which can be detected by BCI.

Since external stimuli for eliciting ERPs can be visual, auditory, and tactile, different types of stimuli have been previously tested for ERP-based BCI control. Most used is the visual modality while the auditory modality is not widely used because of its susceptibility to environmental interferences and relatively low accuracy [1]. The tactile BCIs are not as well-studied probably due to the need for a dedicated stimulation device for ERP eliciting which is more complicated than using a computer screen, light source or a speaker [3].

In this paper, we present an experimental, proof of concept platform of an (electro)tactile BCI based on EEG measurements of somatosensory evoked potentials (SEP) elicited by transcutaneous electrical stimulation (ES) of nerves/muscles.

Marija Novičić – School of Electrical Engineering, University of Belgrade, Bulevar kralja Aleksandra 73, 11000 Belgrade, Serbia (e-mail: novicic@etf.com).

Vera Miler-Jerković – Innovation Center, School of Electrical Engineering, University of Belgrade, Bulevar kralja Aleksandra 73, 11000 Belgrade, Serbia (e-mail: vera.miler@etf.rs)

Olivera Đorđević – Faculty of Medicine, University of Belgrade, Dr Subotica 8, 11000 Belgrade, Serbia (e-mail: odordev@eunet.rs).

Ljubica Konstantinović – Faculty of Medicine, University of Belgrade, Dr Subotica 8, 11000 Belgrade, Serbia (e-mail: ljkonstantinovic@yahoo.com).

Andrej M. Savić – School of Electrical Engineering, University of Belgrade, Bulevar kralja Aleksandra 73, 11000 Belgrade, Serbia (e-mail: andrej_savic@etf.com)

II. Methods

A. Subjects

One healthy male right-handed volunteer (aged 25) participated in this study. He was without a history of neuromuscular disease and with normal vision and had no previous experience with EEG measurements or proof of concept BCI platform. The study was approved by local ethical committee.

B. Instrumentation and experimental setup

The EEG signals were acquired using the g.USBamp amplifier (g.tec GmbH, Austria) in combination with active (g.GAMMAcap2 connected to g.GAMMAbox, g.tec GmbH) at six recording sites for EEG electrodes arranged according to the 10–20 system: FP1, C3, Cz, C4, CP5 and P3. The reference electrode was placed on the left earlobe and the ground was at the location AFz. FP1 location was used to register eye-movement artifacts. The signals were digitized with a 1200 Hz sampling rate and the amplifier was configured to use Notch embedded filtering with cut-off frequency of 50 Hz.

The electrical stimulation was delivered by an eight-channel electrical stimulator, MOTIMOVE (3F – Fit Fabricando Faber, Serbia). This stimulator is fully programmable and allows the change of stimulation parameters such as stimulus amplitude, pulse width and frequency of stimulation and in the case of our proof of concept BCI platform the parameter settings were made by sending commands from PC via USB. The stimulator has an internal battery power supply which allows mobility and isolation from the main supply.

In order to deliver necessary sensory stimuli, 2 stimulation channels were used. One channel is used for electrical stimulation of dorsal surface (stimulus location D), and the other of volar surface (stimulus location V) of the right forearm. Common indifferent electrode for both channels was round of 2.5 cm diameter and placed on the volar aspect of the right wrist. Two round active electrodes of 1 cm

diameter were placed over the extensor carpi radialis muscle (D location) and flexor carpi radialis (V location). The stimuli were single pulses (compensated biphasic with exponential discharge current) of 0.25 ms duration of the active phase. Inter-stimulus interval was set to 750 ms.

C. Experimental protocol

The participant was seated in a chair with a computer screen in front of him at a distance of approximately 1 m. To reduce ocular artifacts, the participant was instructed to fix his gaze at a fixation cross in the middle of the computer screen while right arm was resting on the table in front of the subject (Fig. 1).

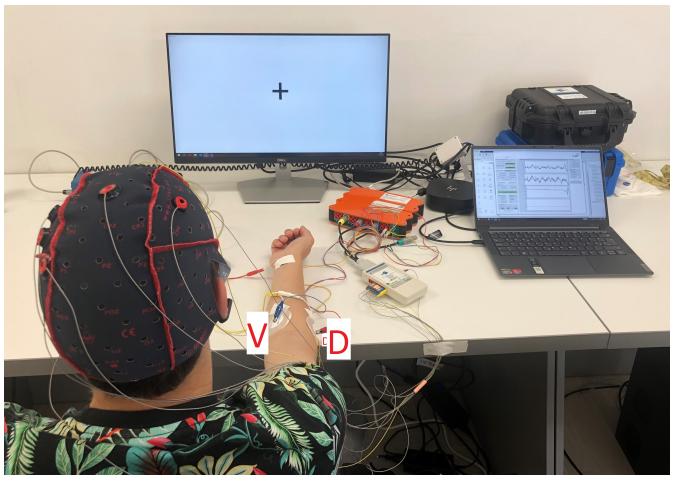

Fig. 1. Experimental setup.

Before the start of the experiment, individual motor threshold was found. Stimulus amplitude was set to 5 mA value and is increased with 1mA step until the contraction was achieved for both D and V locations. The amplitude was then reduced in order to produce the most intense sensation without inducing the contraction. In case of the subject tested those values were 11 mA for D and 10 mA for V.

Experimental protocol was consisted of 6 blocks. Within each block 300 stimuli were delivered in random order to locations D and V while the subject was instructed to attend the stimuli delivered to only one location (D or V) while trying to ignore the stimuli delivered to the other location. The mental strategy in order to maintain the attention was counting the number of stimuli delivered to target location per block. Within blocks 1, 3 and 5 the subject counted the stimuli delivered to location D while in blocks 2, 4 and 6, subject's attention was focused on location V. Therefore, within the duration of the experiment the total number of delivered stimuli was 1800, i.e. 900 per experimental condition (focus on D – F_D, and focus on V – F_V).

D. Software

Graphical user interface (GUI) for stimulation control and data acquisition was developed in MATLAB R2020a (MathWorks Inc., Natick, USA) programming environment (Fig. 2). The GUI consists of four sections.

1) Electrical stimulator control: In this section communication parameters were specified. When communication with stimulator was established, parameters for electrical stimulation were defined. The operator can set value of stimulus amplitude, pulse width and stimulation electrode for both location D and location V. These parameters could be changed during the experiment.

2) Data acquisition: In this section operator needed to set sampling rate and the buffering block size. Sample rate was set to 1200 Hz and buffering block size was set to 60. With these settings, and timer interrupt period, each timer epoch acquires 900 samples.

3) Experiment protocol settings: In this part of the interface operator had to set the parameters that define number of stimuli per block for both channels, number of blocks and duration of pause between blocks. Operator could also choose how the sequence of stimuli was generated. Five options were available: only D is stimulated, only V is stimulated, alternating stimulation between D and V, pseudo random manner with restriction that no more than two consecutive stimuli can be delivered on the same location, and pseudo random manner with restriction that no more than three consecutive stimuli can be delivered on the same location. Finally, operator initialized the session by clicking one of two buttons, depending on which stimulation location the subject has to focus on, so that the dataset was saved and named accordingly to the task (experimental condition).

4) Data visualization: Signals from all channels were shown on the GUI with one of three options. First option showed raw signals. Second one showed signals after filtering with Butterworth 2nd order bandpass filter in a range 1 - 30 Hz. Both first and second option showed signals in time interval of 0.75 s. Third option showed signals of longer duration which was used while preparing the subject for the test and inspecting the EEG signal quality.

E. Data processing

The collected EEG data was bandpass filtered using a 2nd order Butterworth filter in a range 0.1–25 Hz. EEG was segmented to 500 ms epochs (100 ms pre-stimulus baseline and 400 ms post-stimulus interval). Epochs containing artifacts were rejected, where epochs with high absolute amplitude potential shifts (at channels selected for further analysis) and eye-blink/movement artifacts (detected from the Fp1 channel) were selected for rejection. Noise-free epochs were baseline corrected and averaged to form 4 SEP waveforms derived from 2 experimental conditions: 1) focus attention on D while D was stimulated (F_DS_D), 2) focus attention on D while V was stimulated (F_DS_V), 3) focus attention on V while V was stimulated (F_VS_V) and 4) focus attention on V while D was stimulated (F_VS_D). The SEP difference waveforms were calculated by subtracting the SEPs of location D and V delivered within the same condition (task). Namely, difference waveform for FD condition was calculated as F_DS_D-F_DS_V while the difference waveform for F_V condition was calculated as F_VS_D-F_VS_V.

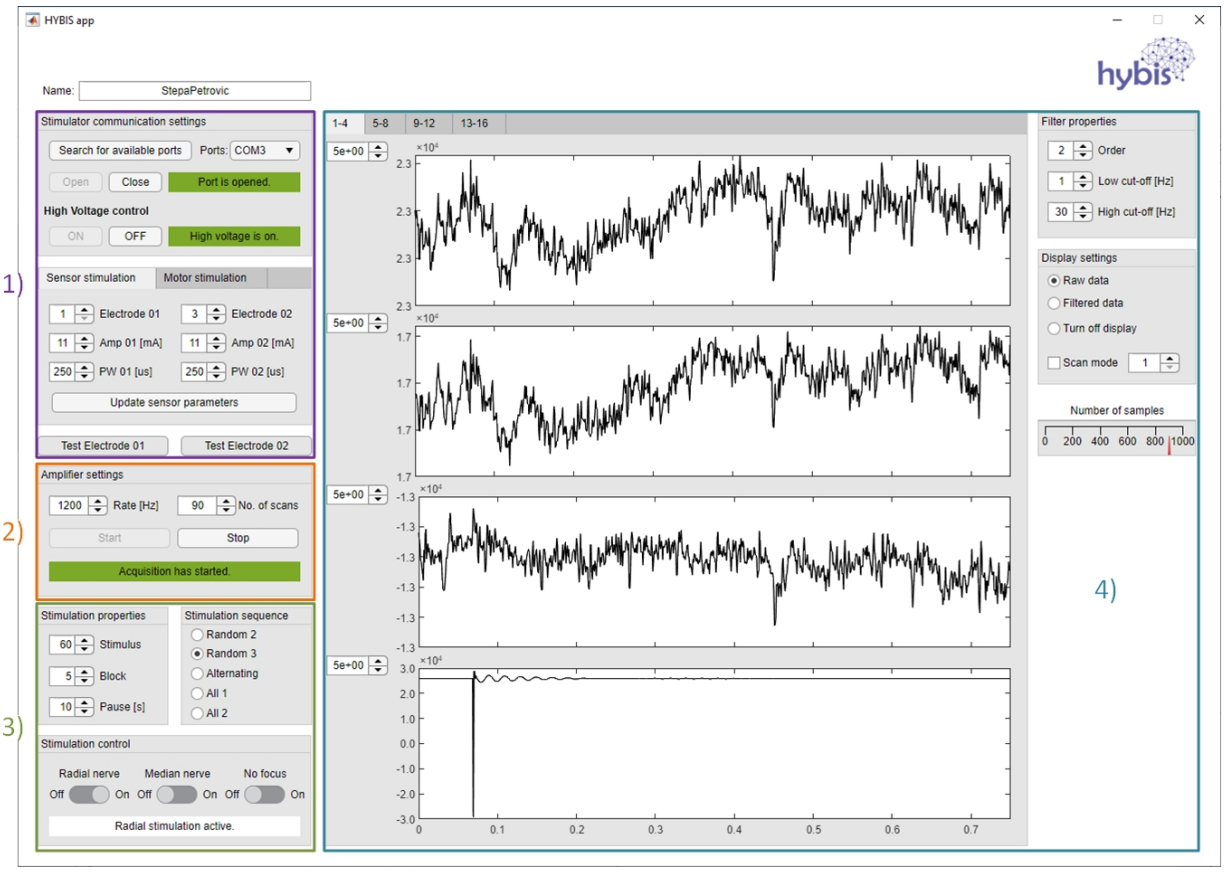

Fig. 2. Main window of the software application GUI during experiment. GUI is divided into four sections: 1) Setting the parameters for communication with electrical stimulator (com port) and stimulation parameters (stimulus amplitude, pulse width and stimulation electrode for both D and V locations), 2) Setting the parameters for data acquisition (sampling rate of acquisition and buffer block size), 3) Setting the parameters for experimental protocol (number of blocks, number of stimuli per block, pause duration and type of sequence), and 4) Data visualisation.

III. Results

SEP waveforms showed that attending the stimuli delivered at one location (D or V) modified the shape of the signal which was reflected in the SEP difference waveform. Representative data for P3 channel is shown in Fig. 3 and 4. Fig. 3 shows the average SEP waveforms when the attention focus was on

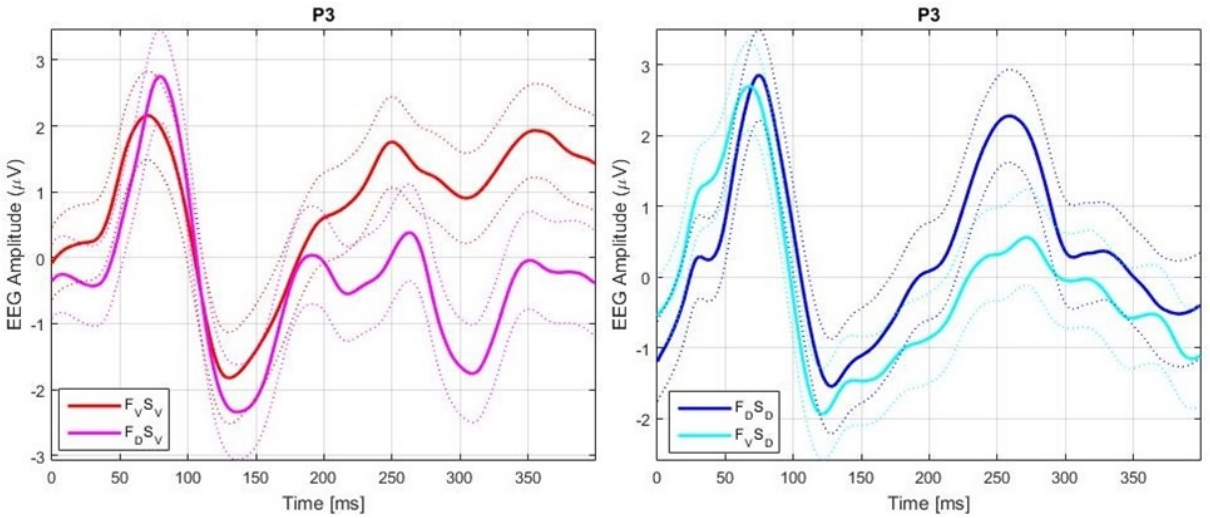

Fig. 3. Left graph shows 2 average SEP waveforms associated with stimulation of dorsal surface of the forearm (SD) while the subject was counting stimuli delivered on dorsal (focus dorsal – F_D, blue line) or volar (F_V , cyan line) surface. Right graph shows 2 average SEP waveforms associated with stimulation of volar surface of the forearm (S_V) while the subject was counting stimuli delivered on volar (focus dorsal – F_V, red line) or volar (F_D, magenda line) surface. Dotted lines present 95% confidence intervals. SEP graphs are presented for EEG channel P3.

the stimulated spot (blue line for D and red for V) or on the other spot (cyan and magenta lines, respectively).

Fig. 4 shows average difference wave between SEP associated with stimulation of dorsal (D) and volar (V) surface of the forearm while the attention focus was on the stimuli delivered to D (blue line) or V (red line).

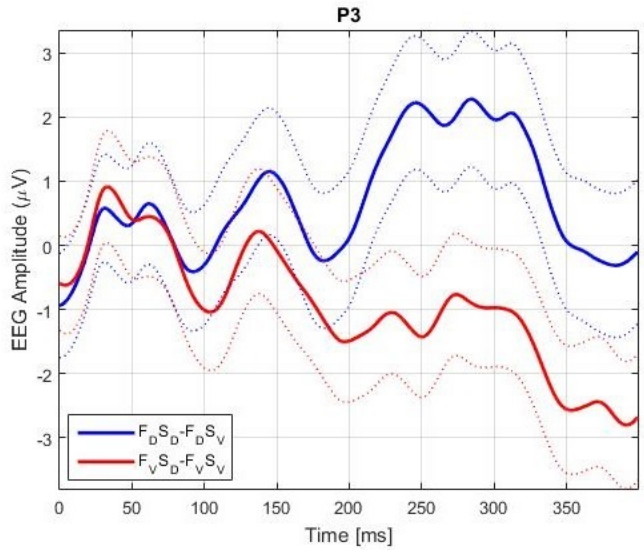

Fig. 4. Blue line represents average difference wave between SEP associated with stimulation of dorsal and volar surface of the forearm while the attention focus was on the stimuli delivered to dorsal surface. Red line represents average difference wave between SEP associated with stimulation of dorsal and volar surface of the forearm while the attention focus was on the stimuli delivered to volar surface. Dotted lines present 95% confidence intervals. SEP graphs are presented for EEG channel P3.

Results indicate significant increase in SEP amplitude of endogenous components, associated with attention focus in both stimulated locations.

IV. Discussion and conclusion

The presented SEP waveforms for both stimulated locations show similar morphology characterized with a first positive component between 50 and 100 ms and negative component between 100 and 150 ms post-stimulus.

Attention focus has resulted in increase of SEP amplitude peaking around 260 ms for SEP associated with D and around 310 ms for SEP associated with V (Fig. 3). The SEP difference waves reveal the window of significance in which the attention focus significantly impacts the processing of somatosensory stimuli in this subject between 210 and 350 ms (Fig. 4) which coincide with P300 ERP component, reflecting the processes involved in stimulus evaluation or categorization [4]. Therefore, our preliminary results validate the SEP recording using our platform and verify that the association of attention focus on SEP amplitude is in a physiologically congruent manner.

This proof of concept platform is a first step towards a novel BCI system for training of somatosensory functions.

Acknowledgment

This work was conducted within project HYBIS funded by the Science Fund Republic of Serbia, under the program for excellent projects of young researchers (PROMIS).

References

[1] C. Chu, J. Luo, X. Tian, X. Han, and S. Guo, "A p300 brain-computer interface paradigm based on electric and vibration simple command tactile stimulation," *Frontiers in Human Neuroscience*, vol. 15, 2021.

[2] A. Rezeika, M. Benda, P. Stawicki, F. Gembler, A. Saboor, and I. Volosyak, "Brain–computer interface spellers: A review," *Brain sciences*, vol. 8, no. 4, p. 57, 2018.

[3] A.-M. Brouwer and J. B. Van Erp, "A tactile p300 brain-computer interface," *Frontiers in neuroscience*, vol. 4, p. 19, 2010.

[4] A. Azizian, A. Freitas, T. Watson, and N. Squires, "Electrophysiological correlates of categorization: P300 amplitude as index of target similarity," *Biological psychology*, vol. 71, no. 3, pp. 278–288, 2006.

Frequency burst modulation outperforms spatial encoding in multi-level vibrotactile stimulation

Nikolina Maravić, Jelena Bulatović, Filip Gašparić, Strahinja Došen, Nikola Jorgovanović

***Abstract*—Haptic or tactile communication refers to communication through touch. Multichannel vibrotactile stimulation is a commonly used interface to provide tactile feedback. The feedback information is delivered to the subject by modulating stimulation parameters. The present manuscript investigates two approaches for encoding of the feedback information. To this aim, two experiments were performed in 20 healthy able-bodied subjects, whose task was to learn to distinguish eight levels of feedback variable using either burst frequency modulation or spatial locations of vibromotor activation. Vibrotactile feedback was delivered through vibration motors placed on the subject's forearm. The experiments consisted of three phases: a familiarization phase, a reinforced learning phase and a validation phase. The main outcome measure was the success rate in discriminating the levels of the feedback variable. The results have shown that burst frequency modulation (72% success rate) outperformed the spatial coding (64%). Therefore, the frequency encoding is the preferred approach in transmitting multilevel feedback information in vibrotactile feedback systems.**

***Index Terms*—vibrations; stimulation; vibromotors; haptic interface; frequency burst modulation; spatial encoding.**

I. Introduction

The sense of touch is one of the most informative senses, and it is instrumental for daily life activities, haptic exploration and social interaction [1]. There are situations in which a person cannot receive tactile information from the environment, for example, in the case of teleoperation or prosthesis use. In these cases, the missing information can be provided through artificially designed haptic feedback [2]. Generally speaking, the term "haptics" refers to the two types of feedback: feeling of touch on the skin and kinesthetic feedback [3]. Kinesthetic sensations are generated by the sensors located within the muscles and tendons and they allow person to gain a sense of the position of the limbs in space [4].

Nikolina Maravić is with the Faculty of Technical Sciences, University of Novi Sad, 6 Trg Dositeja Obradovića, 21000 Novi Sad, Serbia (e-mail: nikolina.maravic@uns.ac.rs).

Jelena Bulatović is with the Faculty of Technical Sciences, University of Novi Sad, 6 Trg Dositeja Obradovića, 21000 Novi Sad, Serbia (e-mail: jelena996@uns.ac.rs).

Filip Gašparić is with the Faculty of Technical Sciences, University of Novi Sad, 6 Trg Dositeja Obradovića, 21000 Novi Sad, Serbia (e-mail: filip.gasparic@uns.ac.rs).

Strahinja Došen is with the Department of Health Science and Technology, Aalborg University, Frederik Bajers Vej 7D 9220, Aalborg, Denmark (sdosen@hst.aau.dk).

Nikola Jorgovanović is with the Faculty of Technical Sciences, University of Novi Sad, 6 Trg Dositeja Obradovića, 21000 Novi Sad, Serbia (e-mail: nikolaj@uns.ac.rs).

The haptic interface consists of a real-time display of a virtual or remote environment and a manipulator that represents an interface between the human operator and the simulation (VR) and/or remotely controlled system. The user makes movements within a virtual or remote environment by moving the robotic device and those movements are translated to the simulation and/or remote system. Haptic feedback, which is basically force or touch feedback in a human-machine interface, allows computer simulations of various tasks to convey real, tangible sensations to the user, and objects that are typically visually simulated to assume real physical properties, such as weight, hardness and texture. By incorporating haptic feedback into a virtual or remote environment, users have the ability to interact with objects, rather than just see their representation on a monitor [5].

There are two possible ways to reestablish sensory feedback: invasive, by direct stimulation of the physiologically appropriate neural structures in the peripheral or central nervous system, and noninvasive, by stimulating the skin electrically or mechanically [6]. In both cases, the user needs to learn how to associate the delivered stimuli with events and state of the system (e.g., prosthetic hand, gripper of a tele-manipulated robot).

Sensory feedback systems can be divided into three categories: feedback systems based on sensory substitution, feedback systems based on modality-matched stimulus, and somatotopic feedback systems [7].

Sensory substitution is a method that allows information from the environment to reach the user's body through sensory channels that are not intended for that particular stimulus (for example, replacing the sense of touch with the sense of hearing) or through the same sensory channels but when the stimulus arrives in another form (for example, pressure replaced with vibration) [8]. Most feedback systems use this idea, since it is simple to implement. The leading techniques are vibrotactile and electrotactile substitution, which delivers either mechanical vibrations or electric current to the skin to encode informations from the environment [9].

Vibrotactile feedback is one of the most commonly used solutions. In prosthetics, for instance, vibromotor is often used to produce continuous or discrete vibrations when the prosthesis contacts the object [10–12]. The feedback information (e.g., grasping force) can be conveyed by modulating the stimulus frequency [11–13], amplitude [12] or location [13].

In [14], four questions related to vibrotactile feedback for prosthetic hand control were investigated: optimal location for vibromotors, type of signal that activates them, period after which the feeling of irritation decreases after constant stimulation exposure as well as the effect of feedback on grip

force control. This study confirmed the improvement in grip force control with the help of vibrotactile feedback.

In the experiment described in [15], 18 healthy subjects operated a virtual object using visual and/or vibrotactile feedback. They received informations via vibration on a finger, hand, neck or foot. All subjects had improved performance when vibrotactile feedback was provided.

The performance of 10 amputees during virtual grasping of objects with feedback on hand aperture and force was investigated in [16]. Their task was to capture the object displayed on the computer monitor with a virtual hand, adjusting the aperture of the hand and the force of the grip using computer mouse. The percentage of correctly applied levels of hand aperture and grip force showed that the use of vibrotactile feedback led to an improvement in hand control compared to the control without feedback.

In [17], two experiments were described: the first referred to the spatial discrimination of stimuli, and the second to the observation of different stimulation intensities. By combining three intensities and three durations of vibrotactile stimulation, nine different stimuli were obtained, which were tested using six vibromotors arranged in four different ways. In the first experiment, circularly placed vibromotors around the upper arm with a proportional distance gave the best results with the accuracy of 75%. Another experiment showed that the perception of vibration intensity was affected by both intensity and duration of vibromotor activation. Seven amputees achieved the accuracy of up to 92% with a circular-proportional vibromotor arrangement.

Despite many studies have used vibrotactile stimulation, no comparison of frequency and spatial coding shemes has been introduced so far. In this study, two vibrotactile coding schemes were presented and compared. Both schemes have the same resolution, they encode 8 levels of vibrations. The difference between two methods is that one implies a variable stimulus burst frequency and other implies variable location of stimulus. The novelty is in comparing frequency and spatial coding schemes which have not been presented so far. The quality of the coding schemes was evaluated using an average success rate achieved by 10 subjects in each experiment in distinguishing levels of vibromotor activation.

II. Methods

The aim of the research described in this paper is to find an adequate way for conveying information using vibrotactile feedback. The idea is to use vibromotors which will be activated according to different spatial and frequency coding schemes so that the user can interpret transmitted feedback information as good as possible. To this aim, we have investigated how well able-bodied subjects could distinguish eight levels of vibrotactile feedback when they are conveyed using different locations versus burst frequency of vibromotor activation.

A. Experimental environment

Eight coin type vibration motors (10mm diameter) were installed in the bracelet and placed circumferentially around the subject's forearm, 2 cm below the elbow (Fig. 1). Vibromotors were marked with numbers 1 – 8. Vibromotor marked with the number "1" was placed in the middle of the lateral forearm, while the others were placed equidistantly, in a clockwise direction. The number of used vibromotors varied depending on the experiment that was performed. In the Experiment 1, four vibromotors were used (marked with numbers 1, 3, 5 and 7), while in the Experiment 2 all eight vibromotors were used. They were connected to the custom made driver board developed at the Faculty of Technical Sciences, University of Novi Sad, which was connected to a PC using a USB cable. The MATLAB software package (version R2018a, MathWorks, USA) was used for creating custom scripts to control the board and collect the data.

Figure 1 shows subject during the experiment. The bracelet with built-in vibromotors was placed around the his/her left forearm, while the subject used his/her right hand to control the mouse when getting acquainted with the levels of vibromotor activation, and then to select the assumed patterns of vibromotor activation.

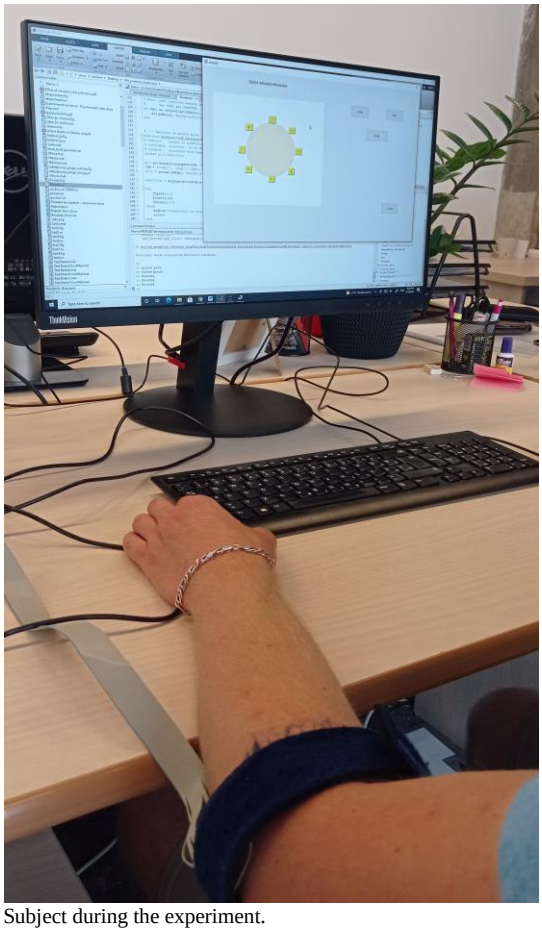

Fig. 1. Subject during the experiment.

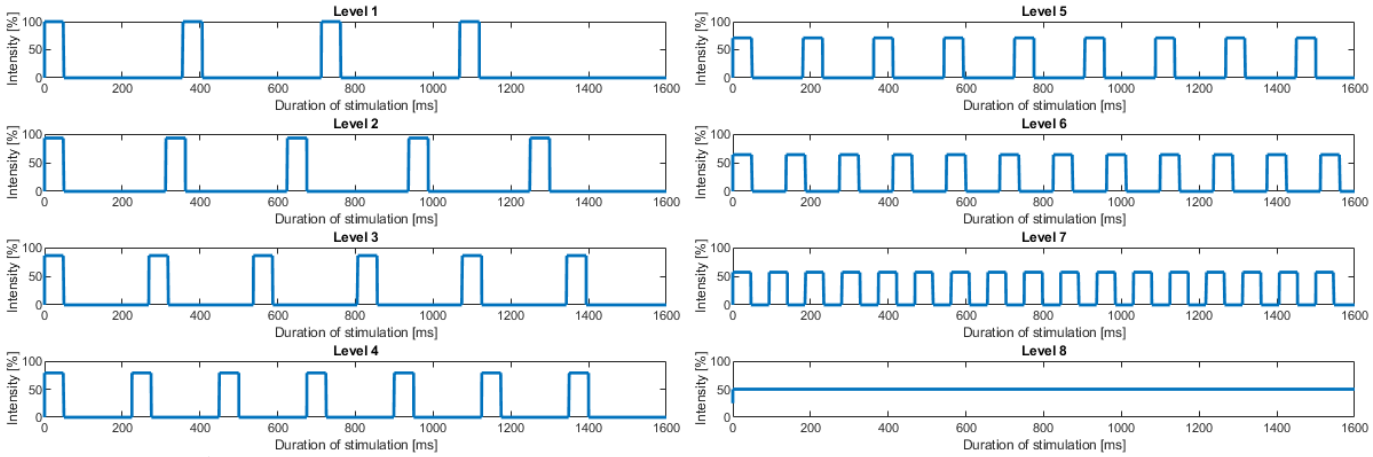

Fig. 2. Control signals for activating vibration motors at eight levels in the Experiment 1.

B. *Stimulation calibration*

Before the beginning of the experiments, it was necessary to determine the parameters of vibrotactile stimulation to create coding schemes that can be clearly perceived by the subjects. For each subject, firstly, the sensation threshold was determined for all vibrators. Each vibromotor was switched on individually, with the vibration intensity gradually increasing from 0 to 100%, in steps of 5%. The intensity at which the subject started feeling vibrations was recorded (sensation threshold).

For the most people the sensation threshold was approx. 30%. Therefore, in the Experiment 1 the intensity of vibrations was obtained by dividing the range between 50% and 100% to eight equidistant values. Remaining stimulation parameters for Experiment 1 were determined after a series of pilot tests. The total duration of stimulation was set to be 1600 ms during which the vibromotors were activated periodically, with an active stimulation ("ON") period of 50 ms. The length of the "OFF" period depended on the level of stimulation and was obtained by dividing the range from 50 to 400 ms by eight equidistant values (Fig. 2). The perceived intensity of vibromotor activation also depends on the length of the stimulation period. By reducing the period of stimulation, i.e. by increasing the frequency with which the stimulus appears, perceived intensity is increasing. However, by adjusting the intensity so that it gradually decreases with increasing burst frequency, the perceived intensity of vibrations can be made approximately equal at each level. When the frequency of stimulus occurrence is the lowest, the stimulation intensity is set to be the highest, i.e. 100% of the maximum value of the simulation, and this pattern was associated to the first level of hypothetical feedback variable. By testing different intensities, it was determined that, when burst frequency is the highest, the activation intensity should be reduced to 50% of the maximum - this corresponded to the eighth level of feedback variable. Figure 2 illustrates the control signals which activate vibromotors. As explained above, the designed patterns produce sensations that modulate in frequency while maintaining approx. the same intensity. Within the pilot tests, the configurations with 1 and 4 equidistantly arranged vibromotors were tested. Subjects reported that the different frequency levels can be distinguished better in the case of using 4 vibromotors. According to that, during the Experiment 1 at a time all four vibration motors were activated simultaneously.

In the Experiment 2, vibrotactile stimulation was delivered through 8 vibration motors equidistantly arranged around the forearm as shown in Figure 3. The vibration intensity was constant and set to 35% to assure that the sensations can be clearly perceived by the subject and yet limit the spread of sensations between adjacent vibrators Only one vibration motor was active at a time. In each trial, the vibromotor was activated for 1000 ms.

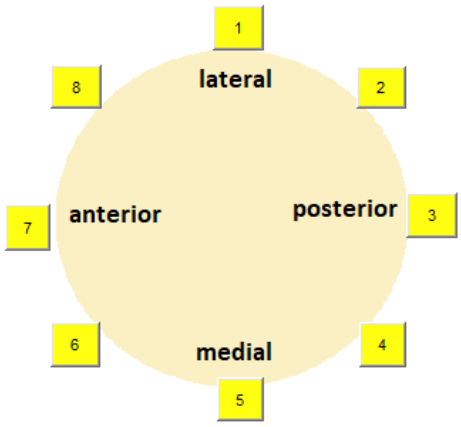

Fig. 3. Locations od vibromotors in the Experiment 2.

C. *Experimental protocol*

The procedure for both experiments was the same and the only difference is that patterns in one case are burst frequency modulations and in the other individual vibrations at different locations. Experimental procedure comprising three phases: the familiarization phase, the reinforced learning phase and the validation phase. Experiments are organized as follows:

1) Familiarization phase

During the familiarization phase, the subject was introduced to the experimental environment and to the sensations elicited by different patterns of vibromotor activations. The familiarization phase was finished when the subject was able to distinguish eight patterns of vibromotor activation.

2) Reinforced learning phase

In the learning phase, the vibromotors were activated at different patterns in random order. The subject guessed the value of the activation level after stimulation, and after selecting the answer, the actual value of the level was shown on a computer screen. Each pattern was activated three times in case of frequency coding and ten times in case of spatial coding.

3) Validation phase

The validation phase followed the same protocol as the learning phase, but without feedback information about the correct answer. Validation phase during the Experiment 1 consisted of 25 trials, which means each level appears at least three times (7 levels appears 3 times and 1 level appears 4 times as a task). Experiment 2 consisted of 80 trials, so each location of vibromotor appears 10 times. After 25 (Experiment 1) or 80 (Experiment 2) stimulations, the test phase was completed.

D. Subjects

The subjects in the experiments were professors, assistants and students from the Department of Automation and Computer Science at the Faculty of Technical Sciences, University of Novi Sad. The Experiment 1 was performed in 10 healthy subjects, seven women and three men; aged 29 ± 11 years (mean ± standard deviation), and the Experiment 2 was performed in 10 healthy subjects, six women and four men; aged 31 ± 12 years (mean ± standard deviation). All subjects signed a written consent form to participate in the experiment.

E. Data analysis

During the validation phase, data containing true and predicted values of the location and level of activated vibromotors were collected. The subject had the role of a classifier who had the task to classify each sample, i.e. stimulus into one of the eight possible classes. Here the classes represent the levels of activation of the vibromotor in the first experiment, i.e. locations of activated vibromotors in the second experiment. From the collected data, confusion matrices were formed for each subject. Each row of the matrices represents an actual class, while each column represents a predicted class. All correct predictions are located in the diagonal of the confusion matrices. Based on these matrices, subject's success rates were calculated as percentage of correct answers among a number of all attempts.

The Kolmogorov-Smirnov test was used to check if data came from a normal distribution. Because of data are not normally distributed, the Mann-Whitney U-test was performed in order to compare two coding approaches. The Mann-Whitney U-test tested the null hypothesis that success rates obtained in two independent experiments are samples from continuous distributions with equal medians. Considering the *p*-value is 0.2716 we cannot conclude that there is enough evidence to reject the null hypothesis and can conclude that a positive shift in the medians of observed data exists.

III. RESULTS

From the collected data, confusion matrices were formed for each subject. Overall confusion matrices for both experiments were calculated as sum of confusion matrices for all subjects. The performance in recognizing vibration patterns is summarized in Fig. 4 in the form of overall confusion matrices with normalized success rates for all levels.

In Experiment 1, the subjects had the highest success rate in recognizing levels one, two, three and eight, while they were less successful in recognizing other levels. They made the most mistakes in recognizing the fifth level and in distinguishing between levels six and seven. It was easiest for them to recognize level eight, which was expected, considering that in this case the vibromotors were activated continuously for 1600 ms. Also, subjects report that the first, second and third level could be most easily distinguished by simply counting the pulses, since the pulses occur with a frequency low enough to count them.

In Experiment 2, most of the mistakes were confined to adjacent vibromotors. The highest success rate in localizing vibrotactile stimulation was achieved on the lateral side of forearm (vibromotors marked with numbers "1", "2" and "8" in Figure 3). The lowest success rate in localizing vibrations was achieved on the posterior side of forearm - vibromotor marked with number "3".

Average success rate for all levels in Experiment 1 is 72%, while in Experiment 2 it is 63%. Therefore, it can be concluded that better results were achieved when feedback variable in vibrotactile systems is stimulus burst frequency than spatial location of the stimulus.

IV. DISCUSSION

A comparison of frequency burst modulation and spatial encoding of vibrotactile stimulation was presented. Twenty healthy subjects participated in two experiments. Effectiveness of each coding scheme was evaluated using success rate achieved in distinguishing eight different levels. Depending on the experiment, stimulus frequency or location was modulated. In the Experiment 1 four vibration motors were activated simultaneously with variable stimulus frequency, while in the Experiment 2 at a time one of eight vibration motor was activated and subject's task was to localize it. Better results in distinguishing eight different patterns were achieved in case of using frequency coding scheme.

The obtained results make a contribution to the field of haptic interfaces. Vibrotactile stimulation is simple to implement and it allows informations from the environment to reach the user's body through mechanical vibrations. In hand prosthetics, for instance, vibration pattern can be used for identifying the prosthesis contact with the object, or level of grip force.

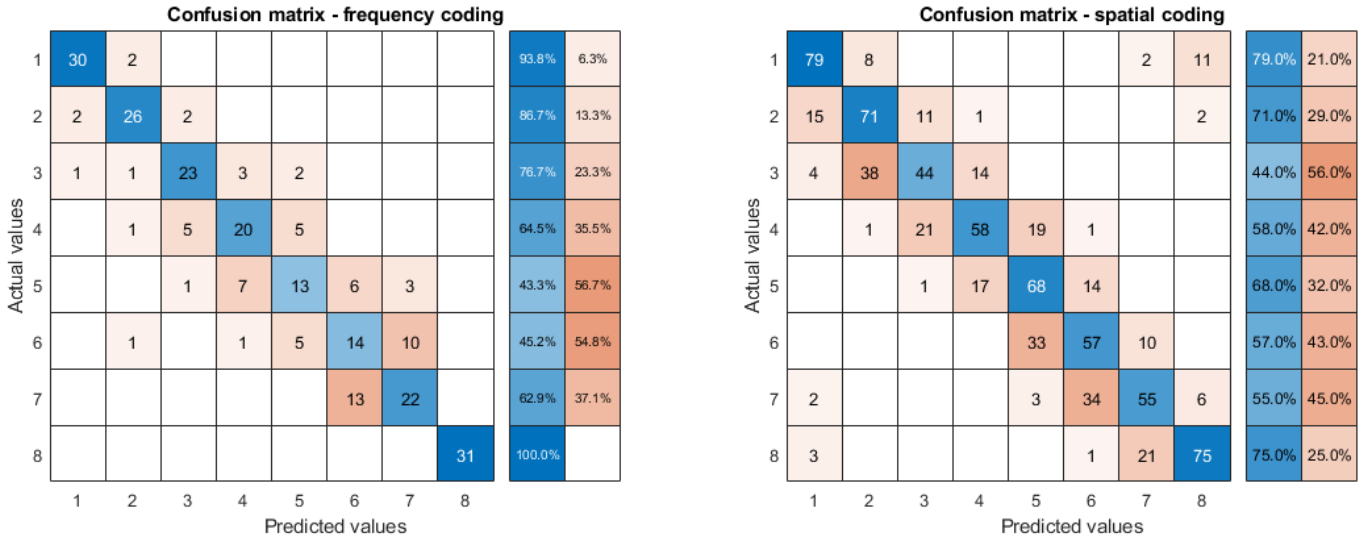

Fig. 4. Overall confusion matrices for both experiments.

V. Conclusion

High performance achieved in described experiments indicate that the frequency and spatial coding schemes of the vibromotor activation are intuitive to use, and they could be applied for providing vibrotactile feedback about 8 levels of feedback variable. However, the frequency burst approach outperformed the spatial encoding. Most of the mistakes made by the subjects involve adjacent levels.

Several female subjects characterized the feeling of vibration on the skin as unpleasant, especially when activating vibromotors at higher frequency levels (6, 7 and 8) during the Experiment 1. The reason for this may be that women's skin is thinner, more moist and covered with less hair, as well as the smaller volume of a woman's forearm compared to a man's, and the intensity of vibration felt in this case is higher. This problem can be solved by adjusting the vibration intensity before starting the experiment for each subject separately.

VI. Acknowledgment

This research was supported by the grants III41007 from the Ministry of Education, Science and Technological development of Serbia.

References

[1] O'malley, M.K. and Gupta, A., 2008. Haptic interfaces. *HCI beyond the GUI: Design for Haptic, Speech, Olfactory, and other nontraditional Interfaces*, pp.25-64.

[2] Brown JD, Paek A, Syed M, O'Malley MK, Shewokis PA, Contreras-Vidal JL, Davis AJ, Gillespie RB: Understanding the role of haptic feedback in a teleoperated/ prosthetic grasp and lift task. *World Haptics Conf* 2013:271–276.

[3] Tzafestas, C.S.: Whole-Hand Kinestethic Feedback and Haptic Perception in Dextrous Virtual Manipulation, *IEEE Transactions on Systems, Man, and Cybernetics - Part A: Systems and Humans*, Vol. 33, No. 1, 2003.

[4] Proske U, Gandevia SC (2018) Kinesthetic Senses. *Compr Physiol* 8:1157–1183.

[5] H. Culbertson, S. B. Schorr, and A. M. Okamura, "Haptics: The present and future of artificial touch sensation," *Annu. Rev. Control, Robot., Auton. Syst*., vol. 1, pp. 385–409, 2018.

[6] S. J. Bensmaia, D. J. Tyler, and S. Micera, "Restoration of sensory information via bionic hands," *Nat. Biomed. Eng*., pp. 1–3, Nov. 2020.

[7] Schofield, J. S., Evans, K. R., Carey, J. P., and Hebert, J. S. (2014). Applications of sensory feedback in motorized upper extremity prosthesis: a review. *Expert Rev. Med. Devices* 11, 499–511.

[8] Antfolk, C. et al. Sensory feedback in upper limb prosthetics. *Exp. Rev. Med. Dev*. 10, 45–54 (2013).

[9] Kaczmarek, K.A., Webster, J.G., Bach-y-Rita, P. and Tompkins, W.J., 1991. Electrotactile and vibrotactile displays for sensory substitution systems. *IEEE transactions on biomedical engineering*, *38*(1), pp.1-16.

[10] Pylatiuk, C., Kargov, A. and Schulz, S., 2006. Design and evaluation of a low-cost force feedback system for myoelectric prosthetic hands. *JPO: Journal of Prosthetics and Orthotics*, *18*(2), pp.57-61.

[11] Chatterjee, A., Chaubey, P., Martin, J. and Thakor, N., 2008. Testing a prosthetic haptic feedback simulator with an interactive force matching task. *JPO: Journal of Prosthetics and Orthotics*, *20*(2), pp.27-34.

[12] Stepp, C.E. and Matsuoka, Y., 2011. Vibrotactile sensory substitution for object manipulation: amplitude versus pulse train frequency modulation. *IEEE Transactions on Neural Systems and Rehabilitation Engineering*, *20*(1), pp.31-37.

[13] Cholewiak, R.W. and Collins, A.A., 2003. Vibrotactile localization on the arm: effects of place, space and age. *Perc Psychoph* 65:1058- 1077.

[14] Chaubey, P., Rosenbaum-Chou, T., Daly, W. and Boone, D., 2014. Closed-loop vibratory haptic feedback in upper-limb prosthetic users. *JPO: Journal of Prosthetics and Orthotics*, *26*(3), pp.120-127.

[15] Stepp, C.E. and Matsuoka, Y., 2011. Object manipulation improvements due to single session training outweigh the differences among stimulation sites during vibrotactile feedback. *IEEE Transactions on Neural Systems and Rehabilitation Engineering*, *19*(6), pp.677-685.

[16] Witteveen, H.J., Rietman, H.S. and Veltink, P.H., 2015. Vibrotactile grasping force and hand aperture feedback for myoelectric forearm prosthesis users. *Prosthetics and orthotics international*, *39*(3), pp.204-212.

[17] Guemann, M., Bouvier, S., Halgand, C., Paclet, F., Borrini, L., Ricard, D., Lapeyre, E., Cattaert, D. and de Rugy, A., 2019. Effect of vibration characteristics and vibror arrangement on the tactile perception of the upper arm in healthy subjects and upper limb amputees. *Journal of neuroengineering and rehabilitation*, *16*(1), p.138.

Feasibility Test of Activity Index Summary Metric in Human Hand Activity Recognition

Jelena Medarević, Marija Novičić, Marko Marković

***Abstract*— Activity monitoring is a technique for assessing the physical activity that the person undertakes over some time. Activity Index is a metric that summarizes the raw measurements from tri-axial accelerometers, often used for measuring physical activity. Our research compared the Activity Index summary metric for different activity groups and hand usages. We also tested the feasibility of the use of this parameter as a classification feature. Data acquisition was done with previously developed system that includes two smartwatches (one on each wrist) and a smartphone placed in the subject's pocket. Raw data from smartwatch accelerometers was used for the analysis. We calculated the Activity Index for labelled data segments and used ANOVA1 statistical test with Bonferroni correction after data normality was determined by the Lilliefors test (modification of the Kolmogorov-Smirnov test). Significant differences were found between cases of hand usage (left, right, none, both) and between some of the activity groups (walking, sitting standing, grasping, pouring, drinking, opening and closing cupboard, and closing bottle), respectively.**

***Index Terms*—Activity Index, accelerometry, smartwatches, ANOVA1, Wilcoxon rank-sum**

Jelena Medarević is with the School of Electrical Engineering, University of Belgrade, 73 Bulevar kralja Aleksandra, 11020 Belgrade, Serbia (e-mail: mj203110m@student.etf.bg.ac.rs).

Marija Novičić is with the School of Electrical Engineering, University of Belgrade, 73 Bulevar kralja Aleksandra, 11020 Belgrade, Serbia (e-mail: novicic@etf.bg.ac.rs).

Marko Marković is with the Applied Rehabilitation Technology Lab, University Medical Center Göttingen, Von-Siebold-Str. 3, D – 37075 Göttingen, Germany (e-mail: marko.markovic@bccn.uni-goettingen.de)

Speech vs. Music Classification Based on EEG Spectral Features Using Artificial Neural Networks

Ivan Vajs, Predrag Jekić, Aleksandra Marjanović, Milica M. Janković

***Abstract*—The response mechanisms to different neural stimuli are a challenging task in neuroscience research. The auditory activity (response to music, speech, noise, etc.) can cause various emotional and cognitive responses. The neural responses to speech and music are of particular significance since they are almost constantly present in day-to-day life. We present the classification of the reactions to speech and music based on the spectral EEG features. The mean values of four frequency intervals (corresponding to the theta, alpha, beta, and gamma rhythms) were assessed for seven brain regions. These features were then used as the inputs to the classification based on logistic regression and artificial neural networks; both were used to analyze each subject individually and all available data. Feature selection was also performed, and the classification algorithms were trained using all, a half, and a quarter of the features for comparing their importance and variance for each individual and the entire dataset. The best classification accuracy for a single subject was 85.8%, and an accuracy of 67.1% was achieved for all subjects. This result is promising and calls for the analysis of a larger dataset.**

***Index Terms*—EEG; artificial neural networks; logistic regression; classification; feature selection.**

I. Introduction

The analysis of the neural responses to different stimuli is quite widespread in the neuroscience research [1]. One area of interest is the analysis of the relationship between the different types of auditory stimuli and brain activity. More specifically, speech and music are found to be of particular significance, as they are present in all cultures and play an important role in everyday life.

Different modalities can be used to track a person's neural response, with the three most commonly used being electroencephalography EEG [2], magnetoencephalography (MEG) [3] and functional magnetic resonance imaging fMRI [4]. These modalities measure the electrical neural activity, magnetic byproducts of neural activity, the changes related to blood flow, respectively, and are used in a wide range of studies regarding the functional analysis of the brain.

In [5], the authors explored the neural response of 15 subjects when exposed to, and when anticipating audio stimuli. The stimuli were selected to either be neutral, or to induce positive or negative emotions and the response was tracked using MEG. Each stimuli category was preceded with a cue tone of a different frequency so that the subject could know what emotion the following stimuli was meant to induce. It was shown that the brain response was different during the exposure to emotion inducing as opposed to neutral sounds, and that the response of a given stimuli was similar to the response elicited by its corresponding cue tone.

An investigation was carried out in [6] to determine whether neural separability between music and speech response could be detected. There were 47 participants that took part in the experiment and fMRI recordings were made during the exposure to short music excerpts and human vocalizations in a pseudo-random order. The results have shown that there is a specific brain region (a region within the anterior superior temporal gyrus) that responds more strongly to music than voice stimuli.

In [7], a study was conducted with the goal of classifying different musical notes based on the EEG response. Five participants took part in the experiment and the event-related spectral perturbation features were extracted and used as the input to the support vector machine classifier. The results of the study showed a 70% classification accuracy for 12 different classes (notes).

The classification of auditory stimuli (English vowels "a", "i" and "u") was conducted in [8]. Eight subjects took part in the experiment and a recurrent neural network combined with Ben's Spike Algorithm encoding was implemented to classify the EEG signals. The accuracy of 83.2% was obtained when using all 64 available electrodes, and an accuracy of 81.7% when using only 10 of the electrodes.

A classification of speech and music audio recordings was performed in [9]. Although not based on neural response, this paper is interesting because it implemented a novel Spectral Peak Tracking approach applied to the audio recording itself, to

[1]van Vajs is with the School of Electrical Engineering, University of Belgrade, and the Innovation Center, School of Electrical Engineering in Belgrade, Bulevar kralja Aleksandra 73, 11120 Belgrade, Serbia (e-mail: ivan.vajs@ic.etf.bg.ac.rs).

Predrag Jekić is with the School of Electrical Engineering, University of Belgrade, Bulevar kralja Aleksandra 73, 11120 Belgrade, Serbia (e-mail: jp205002p@student.etf.bg.ac.rs).

Aleksandra Marjanović is with the School of Electrical Engineering, University of Belgrade, Bulevar kralja Aleksandra 73, 11120 Belgrade, Serbia (e-mail: amarjanovic@etf.bg.ac.rs).

Milica M. Janković is with the School of Electrical Engineering, University of Belgrade, Bulevar kralja Aleksandra 73, 11120 Belgrade, Serbia (e-mail: piperski@etf.rs).

differentiate between music and speech. Very high classification accuracies (above 99%) achieved using deep learning techniques have shown that the complex structure of music and speech can be differentiated quite well.

Considering that there seems to be neural overlap between the brain response to music and speech [10], effectively distinguishing them using EEG could help separate these responses [11]. This can in turn, aid in the accuracy of the classification of the subjects focus point in the cases of exposure to multiple stimuli, which would be helpful in assistive therapies and the design of hearing loss devices [12].

Although the classification of audio stimuli has been attempted, no study was conducted to differentiate speech and music based on the spectral features of the subject's EEG, using artificial neural networks (ANN).

In this study, the classification of auditory stimuli into two categories (speech and music) was performed using a basic logistic regression model, as well as ANNs. The experiment setup and the EEG processing pipeline, along with the ANN architectures are described in Section II, the results are given in Section III, and the conclusion with directions for future work is given in Section IV.

II. Method

A. Experiment setup

Five healthy participants (Age: 31.4±8.8 years) took part in the experiment. All participants have signed the informed consent. A galvanic skin response (GSR) sensor (Mindfield Biosystems, Gronau, Germany) and an EEG cap (EASYCAP GmbH, Wörthsee, Germany) with 24 electrodes, placed in accordance with the 10–20 system connected to the 24-channel Smarting amplifier (mBrainTrain, Belgrade, Serbia) were used for the recording. Electrode M1 was used as an ECG channel and electrode M2 was excluded from the measurement in order to keep the symmetry of the EEG electrodes. In this study only the EEG signals were taken into consideration, with the sample rate of 256 Hz. The participants were asked to close their eyes and listen to the 30-minute-long audio file containing six sets of recordings trials. Each trial lasted four minutes with a one-minute-long interval of silence beforehand. Three types of audio recordings were played within a trial, each lasting for one minute, separated by 30-second silence intervals. One recording set consists of instrumental music, human speech and bird chirping. A single trial is a random permutation of the three mentioned recording categories. In this study, only the responses to the speech and instrumental music were analyzed. For two of the participants (ID2 and ID3) the measurements from the final third of the experiment were excluded due to the reported discomfort of the participants.

B. EEG processing

Firstly, the recorded EEG signals were filtered using a notch filter to remove the power supply noise at 50 Hz. The EEG corresponding to the music and speech stimuli was cut into data snippets using a time window of two seconds and the time stride of two seconds (i.e., non-overlapping time windows). The data snippet was labeled according to its corresponding stimuli. The feature extraction process was performed on each snippet and consists of the following steps. An estimation of the power spectral density (PSD) was performed electrode-wise, denoted as PSD_e (PSD for electrode e). For every PSD_e, a reference $PSD_{e,ref}$ was extracted from the 10-second interval of silence which precedes the particular stimulus recording. The difference between PSD_e and its respective $PSD_{e,ref}$ (denoted as $PSD_{e,diff}$) was then calculated. At this point, the 22 observed EEG channels (their corresponding $PSD_{e,diff}$) were grouped into 7 categories as follows:

- Frontal left: Fp1, F3, F7, Fz, AFz;
- Frontal right: Fp2, F4, F8, Fz, AFz;
- Central: C3, C4, Cz, CPz;
- Parietal left: P3, P7, Pz, POz;
- Parietal right: P4, P8, Pz, POz;
- Occipital: O1, O2;
- Temporal: T7, T8.

The electrodes were grouped according to their position (frontal, central, parietal, occipital, and temporal), with the frontal and parietal regions being split into two hemispheres, since the number of electrodes in each of the hemispheres was sufficient for them to be observed independently. The $PSD_{e,diff}$ of the electrodes in a single category were averaged, thus creating seven $PSD_{g,diff}$ (PSD for group g, $g \in 1 \div 7$). Finally, the mean spectral power of the following frequency bands (i.e., brainwave activity [13]) was estimated for each $PSD_{g,diff}$:

- [4 Hz, 8 Hz] – theta;
- [8 Hz, 12 Hz] – alpha;
- [12 Hz, 30 Hz] – beta;
- [30 Hz, 80 Hz] – gamma.

This resulted in 4 frequency bands × 7 groups = 28 features for the classification algorithms.

C. Classification algorithms

Multiple models were engineered for the purposes of this study and evaluated using 20-fold cross-validation [14]. In the first part of the study, both a logistic regression (used as a baseline algorithm) and an ANN architecture were designed and trained per participant. The same architectures were used with either 7, 14 or all 28 features as inputs. In the cases of 7 and 14 chosen features, the selection was based on the ANOVA F-value estimated on the training set (Fig. 1.) [15].

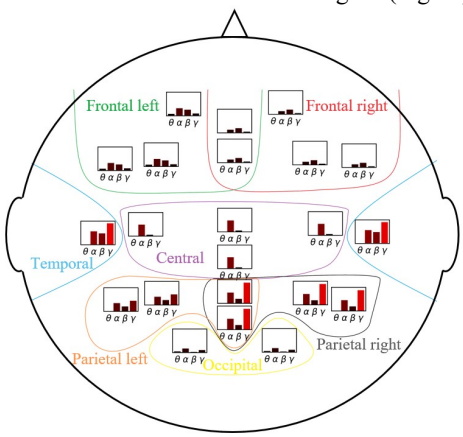

Fig. 1. F-value visualized for each electrode group for a single participant, plotted on the locations of all observed EEG electrodes.

To summarize, there were two different model architectures, three different numbers of input features and five different participants, adding up to 30 different models in total, that were evaluated in this part of the study. In the second part of the study, one logistic regression and three ANN architectures were designed and trained on all collected data, i.e., the data from all participants was placed into a single dataset. These architectures were used for building up different models with either 7, 14 or all 28 features as inputs. Having had four different model architectures and three different numbers of input features, this meant building up 12 different models in total, in the second part of the study.

The shallow ANN used in both the first and second part of the study (ANN1) contained three fully connected (FC) layers (with 5, 4, 2 neurons, respectively). The first hidden layer of ANN1 was a random projection layer, with the purpose of adaptive dimensionality reduction [16]. The other two ANN architectures (ANN2 and ANN3) were evaluated only in the second part of the study. ANN2 contained three FC layers (with 5,10, 2 neurons, respectively). ANN3 consisted of four FC layers (with 5, 15, 10, 2 neurons, respectively). Both ANN2 and ANN3 had a random projection layer as their first hidden layer for the same reason as ANN1. The ANN architectures used for all 28 input features are shown in Fig. 2 (the varying number of input features changes the size of the input layer).

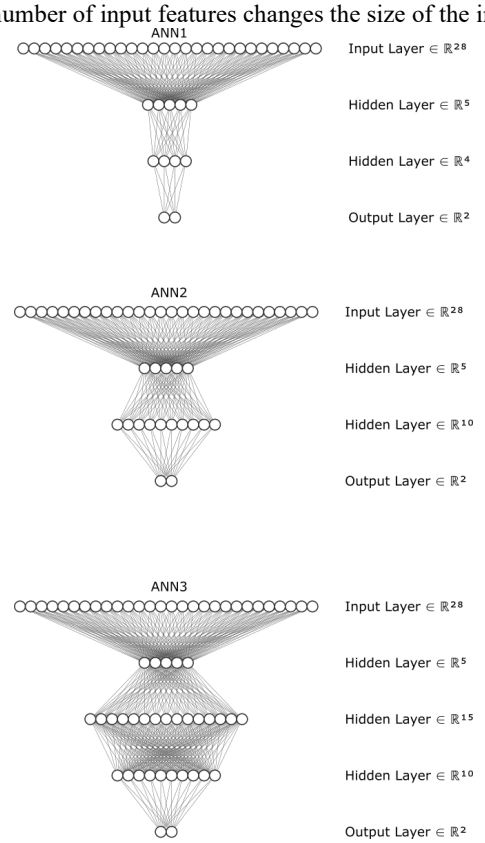

Fig. 2. ANN architectures for all 28 input features.

The relatively low number of neurons and layers was chosen to avoid overfitting considering the dataset size. Adam optimizer was used for the training of the networks with the initial learning rate of 0.00005, batch size of 8, 350 epochs and leaky ReLU activation functions for all hidden layers [17], [18].

III. Results

In Table I, the test classification accuracies are listed per architecture for each subject.

TABLE I
CLASSIFICATION ACCURACY [%] FOR EACH SUBJECT.

	Logistic regression			**ANN1**		
	Number of features			**Number of features**		
ID	28	14	7	28	14	7
1	82.9	78.7	78.4	85.8	81.0	79.7
2	74.5	73.3	65.1	75.2	74.2	67.4
3	81.1	75.1	68.4	84.7	76.2	69.5
4	75.6	72.5	69.5	77.6	73.9	70.1
5	74.3	73.4	71.7	74.9	74.3	72.3

The obtained results show that a higher number of input features corresponds to the higher accuracy regardless of the subject and algorithm (which stands in line with the results from [8]). Furthermore, for a given subject and number of input features, ANN1 consistently achieves a higher accuracy compared to the logistic regression. It is important to note that each subject has their specific features that are consistently selected throughout the cross-validation folds and that these features vary between the subjects (Table II). This is expected due to the natural variation of EEG responses between individuals [19].

TABLE II
THE SELECTED FEATURES FOR EACH PARTICIPANT SHOWN FOR THE TWO FOLDS THAT EXHIBIT THE BIGGEST DIFFERENCE IN FEATURE SELECTION [GROUP NUMBER FOLLOWED BY BRAINWAVE SYMBOL].

ID	**fold**	**14 selected features**	**7 selected features**
1	1	1α, 1β, 2α, 2β, 3α, 4α, 4β, 4γ, 5α, 5β, 5γ, 7α, 7β, 7γ	1α, 3α, 5α, 5γ, 7α, 7β, 7γ
	2	1α, 1β, 2β, 3α, 4α, 4β, 4γ, 5α, 5β, 5γ, 6α, 7α, 7β, 7γ	3α, 4γ, 5α, 5γ, 7α, 7β, 7γ
2	1	2α, 2γ, 3θ, 3α, 3β, 4θ, 5β, 5γ, 6θ, 6α, 6β, 6γ, 7θ, 7γ	2γ, 3θ, 3α, 3β, 5β, 6α, 7γ
	2	1β, 2γ, 3θ, 3α, 3β, 3γ, 5β, 5γ, 6α, 6β, 6γ, 7θ, 7α, 7γ	3θ, 3α, 3β, 4θ, 5β, 6α, 7γ
3	1	1θ, 1β, 2θ, 2α, 2β, 3θ, 3α, 3β, 4β, 4γ, 5α, 5β, 5γ, 6β	3α, 3β, 4β, 4γ, 5β, 5γ, 6β
	2	2θ, 2α, 2β, 3θ, 3α, 3β, 4β, 4γ, 5α, 5β, 5γ, 6θ, 6β, 7α	2θ, 3θ, 3α, 3β, 4γ, 5β, 5γ
4	1	1β, 1γ, 2θ, 2β, 2γ, 3γ, 4α, 4γ, 5α, 5β, 5γ, 6α, 6γ, 7α	1γ, 2γ, 3γ, 4α, 4γ, 5γ, 6α
	2	1β, 1γ, 2θ, 2β, 2γ, 3α, 3γ, 4α, 4γ, 5α, 5γ, 6α, 6γ, 7α	1γ, 2γ, 3γ, 4γ, 5γ, 6α, 6γ
5	1	1θ, 1α, 1γ, 2θ, 2α, 2γ, 3β, 4θ, 4β, 5β, 5γ, 6β, 6γ, 7γ	1θ, 1γ, 2θ, 2γ, 4β, 5γ, 6β
	2	1θ, 1α, 1γ, 2θ, 2α, 2γ, 4θ, 4β, 4γ, 5β, 5γ, 6β, 6γ, 7γ	1θ, 1γ, 4β, 5β, 5γ, 6β, 6γ

In Table III, the test classification accuracies are listed for each model deployed on the set containing the data from all the subjects.

TABLE III
CLASSIFICATION ACCURACY [%] FOR ALL SUBJECTS.

	Number of features		
Architecture	28	14	7
Logistic regression	61.4	59.1	58.3
ANN1	64.8	63.3	62.1
ANN2	65.6	64.2	63.0
ANN3	67.1	64.8	63.9

The overall accuracies shown in Table III are lower than the accuracies obtained when the individual subjects were considered. With respect to the diversity of individual EEG responses and the number of participants it was more difficult for the algorithms to pick up on the complex input-output dependencies.

IV. CONCLUSION

In this paper, the classification of audio stimuli (speech and music) based on spectral EEG features was performed. Firstly, the classification was performed per subject, using the logistic regression and ANN. ANN has shown a slight but consistent improvement (ANN accuracy ranging from 67.4% to 85.8%) over the baseline logistic regression which is to be expected considering the dataset size. Furthermore, a larger number of input features implies a small but consistent increase in accuracy. The deployed models achieved an accuracy above 65% on the test set even when 7 features were selected from the observed dataset. This implies that although a higher number of input features does improve the overall accuracy, certain features do carry more useful information than others. On the other hand, having all collected data in one dataset, resulted in having the maximum accuracy of 67.1%. This is due to the difficulty of achieving higher accuracies when there is an undeniable diversity in the dataset compared to the number of instances and a varying importance of a single feature between subjects.

The directions for the future work include expanding the dataset with significantly more subjects, thus enabling the development of more complex algorithms, alongside the implementation of other EEG processing and feature selection methods. By expanding the database and expanding the EEG feature set, a higher distinction accuracy between speech and music response could be expected. This would open up a possibility to estimate the focus of a given subject when exposed to these stimuli simultaneously, which is often the case in day-to-day life. Further research will also include emotional aspects based on the consideration of heart rate variability (HRV) parameters and the GSR.

ACKNOWLEDGMENT

This research was supported by the Ministry of Education, Science and Technological Development of the Republic of Serbia. The authors would also like to thank all the participants that took part in the experiment and dr Andrej Savić for his useful advice regarding the processing of the EEG signals.

REFERENCES

[1] A. F. Meyer, R. S. Williamson, J. F. Linden, and M. Sahani, "Models of neuronal stimulus-response functions: Elaboration, estimation, and evaluation," *Frontiers in Systems Neuroscience*, vol. 10. Frontiers Media S.A., p. 109, 12-Jan-2017.

[2] C. D. Binnie and P. F. Prior, "Electroencephalography," *Journal of Neurology, Neurosurgery and Psychiatry*, vol. 57, no. 11. BMJ Publishing Group, pp. 1308–1319, 1994.

[3] S. P. Singh, "Magnetoencephalography: Basic principles," *Ann. Indian Acad. Neurol.*, vol. 17, no. SUPPL. 1, p. S107, 2014.

[4] G. H. Glover, "Overview of functional magnetic resonance imaging," *Neurosurgery Clinics of North America*, vol. 22, no. 2. NIH Public Access, pp. 133–139, Apr-2011.

[5] K. Yokosawa, S. Pamilo, L. Hirvenkari, R. Hari, and E. Pihko, "Activation of auditory cortex by anticipating and hearing emotional sounds: An MEG study," *PLoS One*, vol. 8, no. 11, p. 80284, Nov. 2013.

[6] J. L. Armony, W. Aubé, A. Angulo-Perkins, I. Peretz, and L. Concha, "The specificity of neural responses to music and their relation to voice processing: An fMRI-adaptation study," *Neurosci. Lett.*, vol. 593, pp. 35–39, Apr. 2015.

[7] K. Tsekoura and A. Foka, "Classification of EEG signals produced by musical notes as stimuli," *Expert Syst. Appl.*, vol. 159, p. 113507, Nov. 2020.

[8] M.-A. Moinnereau, T. Brienne, S. Brodeur, J. Rouat, K. Whittingstall, and E. Plourde, "Classification of auditory stimuli from EEG signals with a regulated recurrent neural network reservoir," Apr. 2018.

[9] M. Bhattacharjee, S. R. M. Prasanna, and P. Guha, "Speech/Music Classification Using Features From Spectral Peaks," *IEEE/ACM Trans. Audio, Speech, Lang. Process.*, vol. 28, pp. 1549–1559, 2020.

[10] I. Peretz, D. Vuvan, M.-É. Lagrois, and J. L. Armony, "Neural overlap in processing music and speech," *Philos. Trans. R. Soc. B Biol. Sci.*, vol. 370, no. 1664, p. 20140090, 2015.

[11] N. J. Zuk, E. S. Teoh, and E. C. Lalor, "EEG-based classification of natural sounds reveals specialized responses to speech and music," *Neuroimage*, vol. 210, p. 116558, Apr. 2020.

[12] M. Ogg, D. Moraczewski, S. E. Kuchinsky, and L. R. Slevc, "Separable neural representations of sound sources: Speaker identity and musical timbre," *Neuroimage*, vol. 191, pp. 116–126, May 2019.

[13] C. S. Nayak and A. C. Anilkumar, *Eeg normal waveforms*. StatPearls Publishing, 2020.

[14] M. Stone, "Cross-Validatory Choice and Assessment of Statistical Predictions," *J. R. Stat. Soc. Ser. B*, vol. 36, no. 2, pp. 111–147, Jun. 1974.

[15] L. Sthle and S. Wold, "Analysis of variance (ANOVA)," *Chemometrics and Intelligent Laboratory Systems*, vol. 6, no. 4. Elsevier, pp. 259–272, 01-Nov-1989.

[16] P. Iwo, Wojcik, "Random Projectionin Deep Neural Networks," University of Science and Technology in Kraków, 2018.

[17] D. P. Kingma and J. Ba, "Adam: A method for stochastic optimization," *arXiv Prepr. arXiv1412.6980*, 2014.

[18] B. Xu, N. Wang, T. Chen, and M. Li, "Empirical evaluation of rectified activations in convolutional network," *arXiv Prepr. arXiv1505.00853*, 2015.

[19] J. Intriligator and J. Polich, "On the relationship between EEG and ERP variability," *Int. J. Psychophysiol.*, vol. 20, no. 1, pp. 59–74, Jun. 1995.

How TV commercials affect attention and memory?

Brana Kostić, Vanja Ković, Vera Miler Jerković and Milica Janković, *Member, IEEE*

***Abstract*— Neuromarketing is an emerging multidisciplinary field that involves neuroscience methodology to estimate the reaction of consumers to marketing activities and the way they affect their decisions. The most used neurophysiological technique for neuromarketing studies is electroencephalography (EEG). We present a pilot EEG signals-based study on four participants. We investigated the effect of selected seven commercials on memorization and attention. Statistical analysis of extracted attention and memorization indices has shown high inter-subject variability. It has also demonstrated a statistically significant difference ($p<0.05$) between participant reactions on commercials on the individual level. Novel metric based on normalized total score of attention index, memorization index and self-assessment was proposed and demonstrated through the comparison of commercials.**

***Index Terms* — neuromarketing, EEG, attention, memory.**

I. Introduction

NEUROMARKETING, a new field of marketing research, has greatly benefited from applying neurophysiological methodology in investigating conscious and unconscious consumer behavior, during the past decade [1, 2]. At the same time, it is overcoming challenges that the traditional metrics used to offer and adding value to the traditional marketing research [3]. Some of the neurophysiological technologies that are used in neuromarketing are: functional magnetic resonance imaging (fMRI, for measuring changes in blood oxygenation and flow that occur as a response to brain activity) [4], electroencephalography (EEG, for measuring electrical activity in the cerebral cortex) [1, 5], eye tracking [6] or various sensors for measuring changes in human physiological condition (e.g., heart rate, respiratory rate, skin conductivity) [7,8]. EEG technology is affordable and with an excellent temporal resolution, so it is the most used neurophysiological technique for marketing studies [1].

The growing literature in this field has unequivocally shown that EEG can be successfully used for research in the field of advertising and neuromarketing. For example, Dimpfel et al. recorded EEG and eye-tracking signals of participants who observed 5 advertisements about banks and concluded that the advertisements affected the observer in a way that the distinct brain regions were activated depending on the type of the emotion evoked whilst the person observed the advertisement [9]. In another EEG study, with 34 participants who observed 5 advertisements, Balconi et al. [10] found a strong correlation between what customers liked and the activation of the dorsolateral prefrontal cortex (DLPFC). In participants who watched commercials, Vecchiato et al. found an asymmetric increase in theta and alpha activity related to the observation of pleasant and unpleasant advertisements, in the left and right hemisphere, respectively [11,12]. More precisely, they found de-synchronization of the left alpha frontal activity, as well as the higher theta activation on the left frontal and pre-frontal areas, if the respondents liked the advertisement. Astolfi et. al. [13] assessed cortical activity in healthy subjects whilst watching TV commercials inserted within a film, using a high-resolution EEG technique, and found highly significant brain activity during the observation of TV commercials, which was mainly concentrated in the frontoparietal parts of the cortex (approximately grouped around Broadman fields 8, 9 and 7).

The goal of this research was to, based on the EEG measurements [14], assess attention and memory indices for each of the commercials presented to the participants in order to rate them according to these markers. We expected that some commercials would score high on the index of memory, some on the index of attention, some on neither of the two indices, and some on both. That way, the practical value of this research would be to point out those advertisements which are better suited for attracting attention vs. those who are memorized better. The second goal was to assess individual differences across participants.

In Section II we have presented the performed methodology: experiment description and EEG data analysis. Furthermore, we have illustrated group and individual statistical results of TV commercials impact on attention and memory, in Section III. Finally, we have given conclusion and plans for the further work in Section IV.

II. The Method

A. Experiment description

Four healthy participants (1 female and 3 males, age: 27.7±7.5 years) participated in the experiment. All participants have signed the informed consent.

Brana Kostić is with the University of Belgrade - School of Electrical Engineering, Bulevar kralja Aleksandra 73, 11120 Belgrade, Serbia (e-mail: branakostic10@gmail.com).

Vanja Ković is with the University of Belgrade, Faculty of philosophy, Laboratory for Neurocognition and Applied Cognition, Čika Ljubina 18-20, 11000 Belgrade, Serbia (e-mail: vanja.kovic@f.bg.ac.rs).

Vera Miler Jerković is with the Innovation Center, School of Electrical Engineering in Belgrade, Bulevar kralja Aleksandra 73, 11120 Belgrade, Serbia (e-mail: vera.miler@etf.rs).

Milica Janković is with the University of Belgrade - School of Electrical Engineering, Bulevar kralja Aleksandra 73, 11120 Belgrade, Serbia (e-mail: piperski@etf.rs).

During the experiment, participants were asked to comfortably sit in front of the computer screen and watch the prepared video. The video consisted of 7 commercials with a 30 s pause (black screen) between them and at the beginning, as well. Commercials were selected from the list of top 2012 commercials in Serbia [15]. We have considered that the advertisements have been shown on TV long ago and that participants do not remember them in detail, so the initial memory effect was negligible. All commercials had approximately same duration and a similar structure, consisting of three parts: 1) story introduction, 2) action and 3) product logo display. The complete video timeline is presented in Table 1.

EEG data acquisition was performed using a 24-channel Smarting amplifier (mBrainTrain, Belgrade, Serbia) connected to Greentek EEG cap (Wuhan Greentek Pty. Ltd, China). Twenty-two monopolar EEG channels were recorded (10/20 locations: Fp1, Fp2, F3, F4, C3, C4, P3, P4, O1, O2, F7, F8, T7, T8, P7, P8, Fz, Cz, Pz, AFz, CPz, POz). The ground was located at FPz and FCz, and it was used as the reference site. The sampling rate was set to 500Hz. The EEG system sent EEG data via Bluetooth to the computer.

At the end of the experiment, participants were asked to subjectively evaluate each advertisement (scale 1 to 5, 5 was the highest mark).

TABLE I
THE VIDEO TIMELINE

No.	Advertisement's name	Duration
	Pause	30 s
1.	"Forever", Carnex	33 s
	Pause	30 s
2.	"Meeting with happiness", State Lottery of Serbia	30 s
	Pause	30 s
3.	"Infostud jobs"	20 s
	Pause	30 s
4.	"LAV beer"	30 s
	Pause	30 s
5.	"Schweeps"	35 s
	Pause	30 s
6.	"JAFFA cakes"	30 s
	Pause	30 s
7.	"Sportingbet"	28 s

B. EEG data analysis

EEG data analysis consisted of 1) EEG preprocessing, 2) extraction of attention and memory indices and 3) statistical data analysis.

EEG preprocessing included FIR filtering in range 2-30 Hz, removing eye-blink artifacts using *Individual component analysis* (*ICA*) method and bandpass extraction of alpha activity (8-12 Hz) in the right frontal (Fp2, F4, F8) and the left frontal lobe (Fp1, F3, F7) and theta activity (4-8 Hz) in the left frontal lobe (Fp1, F3, F7) by a fifth-order Butterworth filter. The flowchart of the EEG preprocessing is presented in Fig. 1.

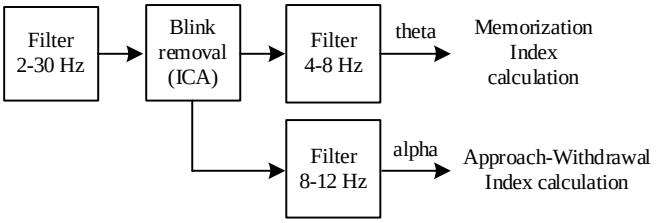

Fig. 1. Flowchart of the EEG preprocessing

Approach-Withdrawal index [7, 8, 16] for attention (*AW*) was calculated on preprocessed alpha activity in the right and left frontal lobes, on time windows of 3 seconds as in

$$AW = P_{\alpha\ right\ frontal} - P_{\alpha\ left\ frontal}$$

$$AW = \frac{1}{N_R}\sum_{i\in R} EEG_{r\,\alpha_i}^2(t) - \frac{1}{N_L}\sum_{i\in L} EEG_{l\,\alpha_i}^2(t) \quad (1)$$

where $P_{\alpha\ right\ frontal}$ and $P_{\alpha\ left\ frontal}$ are the averaged powers of alpha activity in the right and left frontal lobes, respectively; $EEG_{r\,\alpha_i}$ and $EEG_{l\,\alpha_i}$ are the *i*-th preprocessed alpha band EEG channels in the right (R) and left (L) frontal lobes, respectively; N_R and N_L are numbers of $EEG_{r\,\alpha_i}$ and $EEG_{l\,\alpha_i}$ channels (N_R=N_L=3).

Memorization index (*MI*) [17] was calculated on preprocessed theta activity in the left frontal lobe, on time windows of 3 seconds as in

$$MI = P_{\theta\ left\ frontal} = \frac{1}{N_L}\sum_{i\in L} EEG_{l\,\theta_i}^2(t) \quad (2)$$

where $P_{\theta\ left\ frontal}$ is the averaged power of theta activity in the left frontal lobe. $EEG_{l\,\theta_i}$ are the *i*-th preprocessed theta band EEG channels, in the left (L) frontal lobe and N_L is the number of $EEG_{l\,\theta_i}$ channels (N_L=3).

EEG signal preprocessing and indices extraction was done in Matlab R2014b (Mathworks, USA). EEGLAB Toolbox was used for filtering and for *ICA* application [18].

The ANOVA analysis was performed on extracted *AW* and *MI* indices to investigate the statistical differences (the significance values of $p<0.05$) in the reactions of the participants on different commercials. We have analyzed changes in *AW* and *MI* indices on the group level (all participants for each advertisement) and on the individual (participant) level for each advertisement. Statistical analysis was done in RStudio [19]. A novel metric defined as a total score for *AW* index, *MI* index and self-assessment was also calculated (as a sum of participant mean values for each advertisement) and normalized to the range [0,1].

III. RESULTS

Box plots for *AW* and *MI* indices on the participant group level for each commercial is presented in Fig. 2. ANOVA analysis has shown statistically significant difference ($p<0.05$)

between commercials only for *AW* index, Fig. 2A. There was no significant difference between commercials on the participant group level in terms of memory, Fig. 2B.

Individual differences between participants concerning their reaction for each commercial were investigated as well. Fig. 3 shows box plots for *AW* (Fig. 3A) and *MI* (Fig. 3A) indices on the participant level for each advertisement. ANOVA analysis has shown statistically significant difference ($p<0.05$) between commercials for both indices, *AW* and *MI*.

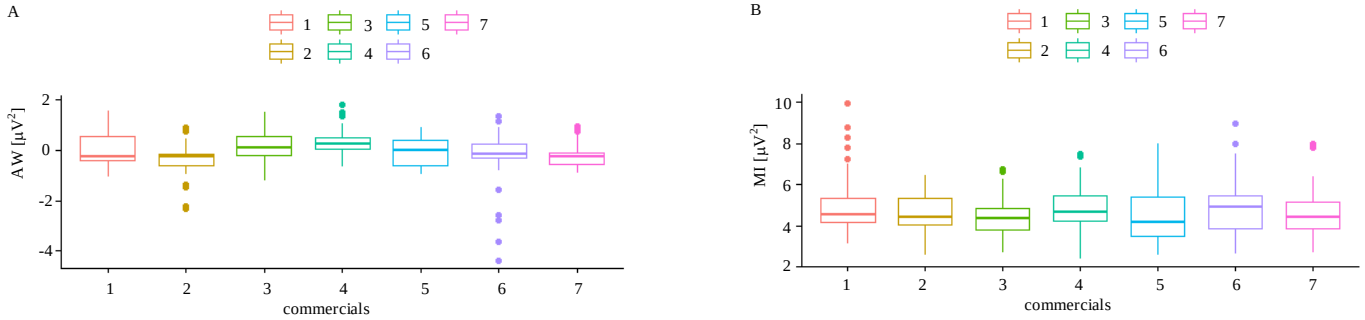

Fig. 2. A) Approach-Withdrawal index (*AW*) and B) Memorization index (*MI*) for each commercial on the participant group level (commercial order 1-7 is shown in Table 1).

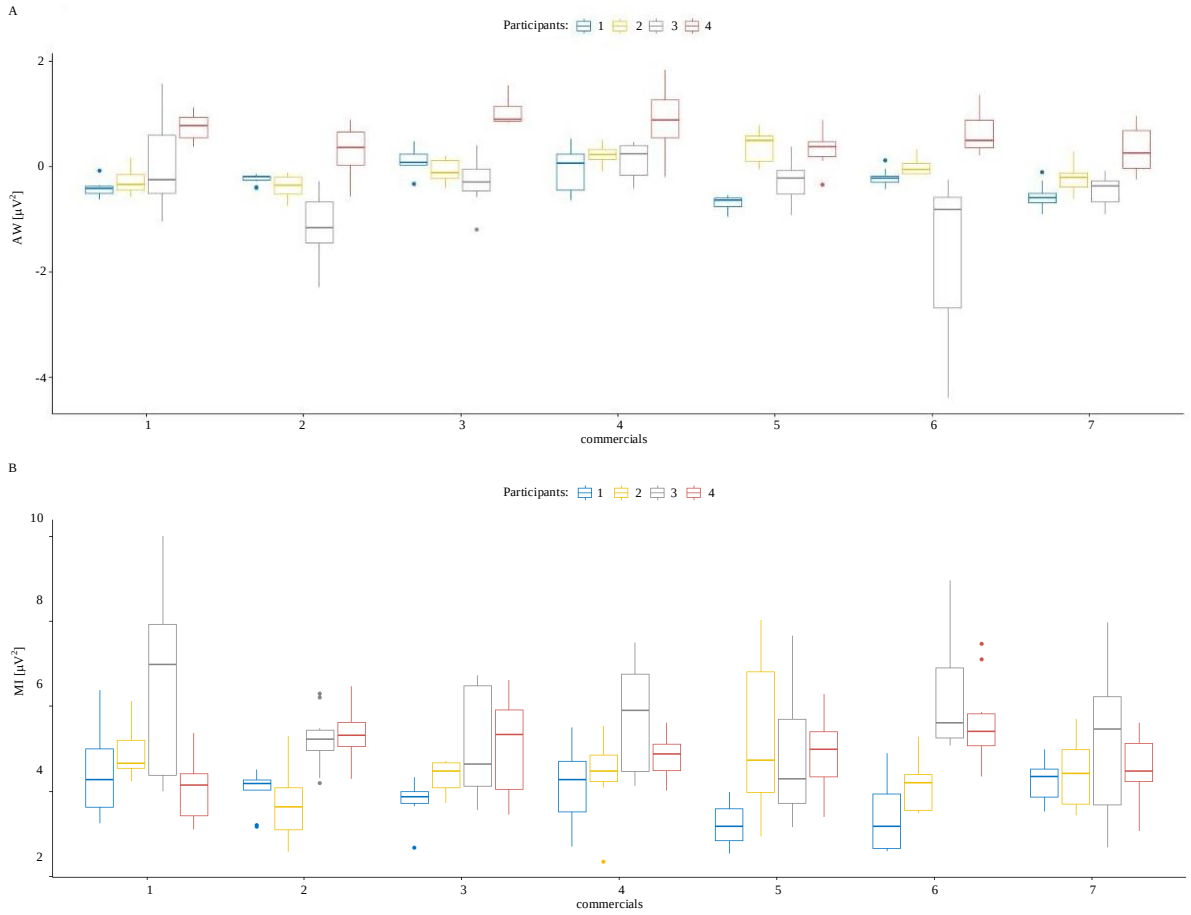

Fig. 3. A) Approach-Withdrawal index (*AW*) and B) Memorization index (*MI*) for each commercial on the individual (participant) level (commercial order 1-7 is shown in Table 1).

From Fig. 3, it can be noticed that there is a high inter-subject variability for each commercial that caused no statistically significant difference for *MI* index on the group level as well as a low statistically significant difference for *AW* index.

Finally, Fig. 4 shows the comparison between normalized total scores of *AW*, *MI* and self-assessment (*SA*) for each commercial. It was found that there is no correlation between *SA* and indices. This means that the objective and subconscious criteria concerning attention and memory is necessary for the detailed observation of the advertisement impact on participants. From Fig. 4, it could be noticed that commercials 1 and 4 have high (attention and memory) impact on participants, commercials 3 and 5 are better suited

to attract attention while commercial 6 was memorized better. It is important to mention that commercial 3 lasts shorter than others (20 s vs 28-35 s) which may be the reason for low memory. Commercials 2 and 7 have low induction of attention and low induction of memory as well. Regarding results presented in Fig. 4, normalized total scoring seems to be a promising tool for comparison and visualization of the effects of advertisements on participants. Potential benefit from this type of analysis is obvious: for the investor, it is important to have objective and detailed feedback from customers regarding their attention and memory engagement whilst watching commercials.

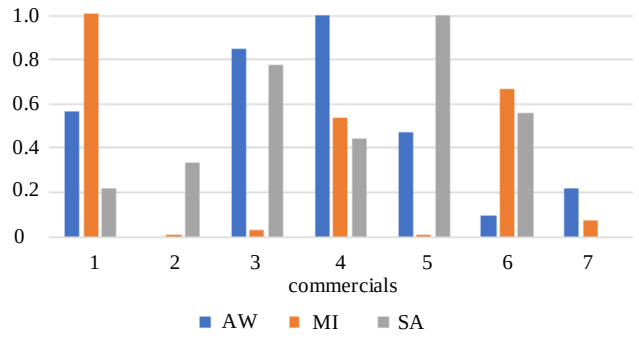

Fig. 4. Comparison of normalized total score for Approach-Withdrawal index (*AW*), Memorization index (*MI*) and Self-assessment (*SA*) for each commercial (commercial order 1-7 is shown in Table 1).

IV. Conclusion

In this paper, we have demonstrated a novel approach for the comparison of commercials in the pilot EEG signals based study. Large individual differences in attention and memory involvement were ascertained between participants whilst watching the video content. For that reason, differences in reactions on commercials for each participant were also considered. Individual approach showed the existence of statistically significant differences for attention and memory indices between commercials. All individual scores for *AW*, *MI* and *SA* were summed and normalized giving an effective way for presenting and comparison of different impacts of commercials on participants. However, this type of neuromarketing study can be expanded by simultaneous recordings of heart rate, electrodermal activity and eye tracking activity (along with EEG signals), enabling the assessment of the emotional index and eye tracking features as well. Also, the longer duration of commercials could enable analyzing and comparing individual parts of advertisement, and not just analyzing advertisements as a whole. Future work will be focused on designing a longer experimental paradigm, applying a multimodal approach for data acquisition and advertising differentiation, using multiparametric analysis.

Acknowledgment

This research was supported by the Ministry for Education, Science and Technology Development of Serbia, Serbia.

References

[1] A. Bazzani, S. Ravaioli, U. Faraguna & G. Turchetti, “Is EEG Suitable for Marketing Research? A Systematic Review”, *Frontiers in Neuroscience*, vol. *14*, pp. *1-16*, 2020.

[2] F. S. Rawnaque, K. M. Rahman, S. F. Anwar, R. Vaidyanathan, T.Chau, F. Sarker, K. A. Al Mamun, “Technological advancements and opportunities in Neuromarketing: a systematic review”, *Brain Informatics*, vol. *7*, no. *1*, pp. *1-19*, 2020.

[3] S. G. Meyerding, C. M. Mehlhose, “Can neuromarketing add value to the traditional marketing research? An exemplary experiment with functional near-infrared spectroscopy (fNIRS)”, *Journal of Business Research*, vol. *107*, pp. *172-185*, 2020.

[4] M.Y.-T Hsu and J.M.-S. Cheng, "fMRI neuromarketing and consumer learning theory: Word-of-mouth effectiveness after product harm crisis", *European Journal of Marketing*, vol. *52* no. *1/2*, pp. *199-223*, 2018.

[5] A. Hakim, I. Golan, S. Yefet, D. J. Levy, “DeePay: Deep Learning Decodes EEG to Predict Consumer’s Willingness to Pay for Neuromarketing”, *TechRxiv*. Preprint, 2021.

[6] B. C. Iloka and G. I. Anukwe, “Review of eye-tracking: A neuromarketing technique” *Neuroscience Research Notes*, vol. 3, no. *4*, pp. *29-34*, 2020

[7] M. Zito, A. Fici, M. Bilucaglia, F. S. Ambrogetti and V. Russo, “Assessing the Emotional Response in Social Communication: The Role of Neuromarketing”, *Frontiers in Psychology*, vol. *12*, pp. *1784-1797*, 2021.

[8] A. C. Martinez-Levy, D. Rossi, G. Cartocci, M. Mancini, G. D. Flumeri, A. Trettel, F. Babiloni, P. Cherubino, “Message framing, non-conscious perception and effectiveness in non-profit advertising. Contribution by neuromarketing research”, *International Review on Public and Nonprofit Marketing*, pp. *1-23*, 2021.

[9] W. Dimpfel, “Neuromarketing: Neurocode-Tracking in Combination with Eye-Tracking for Quantitative Objective Assessment of TV Commercials”, *Journal of Behavioral and Brain Science*, vol. *5* no. *4*, Article ID 55367, pp. *137-147*, 2015.

[10] M. Balconi, B. Stumpo, & F. Leanza, “Advertising, brand and neuromarketing or how consumer brain works,” *Neuropsychological Trends*, vol. *16* no. *2*, pp. *15-21*, 2014.

[11] G. Vecchiato, W. Kong, A. Giulio Maglione, D. Wei, “Understanding the impact of TV commercials” *IEEE pulse*, vol. *3* no. *3*, pp. *42-47*, 2012.

[12] G. Vecchiato, J. Toppi, L. Astolfi, F. D. V. Fallani, F. Cincotti, D. Mattia, F. Bez, & F. Babiloni, “Spectral EEG frontal asymmetries correlate with the experienced pleasantness of TV commercial advertisements”, *Medical & biological engineering & computing*, vol. *49* no. *5*, pp. *579- 583*, 2011.

[13] L. Astolfi, G. Vecchiato, F. De Vico Fallani, S. Salinari, F. Cincotti, F. Aloise, D. Mattia, M. G. Marciani, L. Bianchi, R. Soranzo, F. Babiloni, “The track of brain activity during the observation of tv commercials with the high-resolution EEG technology,” *Computational intelligence and neuroscience*, vol. *2009*, Article ID *652078*, pp. *1-8*, 2009.

[14] B. Kostić, “Quantitative analysis of the impact of advertising on attention and emotions,” master thesis, University of Belgrade – School of Electrical Engineering, Belgrade, Serbia, 2018.

[15] https://www.lumiere.rs/ostalo/istrazivanja/srbija-top-10-srpske-reklame-u-2012-nase-malo-istrazivanje/ [in Serbian] (last access in June 2021)

[16] R. J. Davidson, “What does the prefrontal cortex “do” in affect: perspectives on frontal EEG asymmetry research,” *Biological Psychology*, vol. *67*, no. *1-2*, pp. *219–233*, 2004.

[17] G. Vecchiato, A. G. Maglione, P. Cherubino, B. Wasikowska, A. Wawrzyniak, A. Latuszynska, M. Latuszynska, K. Nermend, I. Graziani, M. R. Leucci, M. Trettel, A. Trettel, “Neurophysiological tools to investigate consumer’s gender differences during the observation of TV commercials”, *Computational and mathematical methods in medicine*, vol. *2014*, Article ID 912981, pp. *1-12*, 2014.

[18] A. Delorme, S. Makeig, “EEGLAB: an open-source toolbox for analysis of single-trial EEG dynamics”, *Journal of Neuroscience Methods*, vol. *134*, pp. *9-21*, 2004.

[19] RStudio Team (2020). RStudio: Integrated Development for R. RStudio, PBC, Boston, MA URL http://www.rstudio.com/.

Open-source tool for 3D segmentation and rendering of abdominal CT scans

Katarina Milićević, Otaš Durutović and Milica Janković, *Member, IEEE*

***Abstract*—3D visualization of the size, shape, and location of the kidney stone as well as of the anatomical characteristics of the renal collecting system, surrounding tissue and blood vessels could significantly facilitate the surgeon's treatment planning for urolithiasis. Standard clinical Computed Tomography (CT) software does not offer the flexibility in the 3D display of individual or combined renal phases. In this paper we present a flexible and interactive open-source application for segmentation and 3D visualization of abdominal CT scans for the urolithiasis treatment planning. The usage of the new tool is demonstrated through the clinical examples and its advantages are explained in comparison with the output of the dedicated clinical software.**

***Index Terms*—abdominal CT, minimally invasive surgery, open-source, 3D rendering, 3D segmentation.**

I. Introduction

THE accurate diagnosis is a prerequisite for the effective treatment [1]. In the era of modern medicine, this assumption becomes more important, since the backbone of quality diagnostics consists of performing radiological procedures, primarily computed tomography (CT) imaging, but also radiography, ultrasound, magnetic resonance imaging (MRI), as well as interventional radiological procedures. Radiological procedures are associated with the patient's exposure to ionizing radiation, and therefore it is necessary to use these procedures rationally and optimally.

Low-dose abdominal CT imaging has high sensitivity, specificity, and accuracy for the detection of urolithiasis (kidney stone disease) [2]. Urolithiasis could be treated conservatively (by pain control, hydration, and medical expulsive therapy), surgically (endoscopic methods: ureteroscopy and percutaneous nephrolithotomy) or by extracorporeal shockwave lithotripsy (shockwaves applied outside the body to break the stone) [3,4]. The size, shape, localization, and structure of the kidney stone determine the decision about the treatment method.

The treatment of choice in case of large stones (>2 cm) or complex anatomic factors is percutaneous nephrolithotomy (PCNL) [5-7]. Each percutaneous (through the skin) path to the kidney and the stone implies the passing of instrument through the renal highly vascularized parenchyma, so the optimization of each puncture, even individual, and kidney access is an imperative for the minimization of potential complications. The prerequisite for the minimally invasive surgery is the detailed 3D visualization of the target organ and its anatomic environment [8].

A reliable anatomical 3D visualization is based on the quality segmentation process. One of the directions for abdominal segmentation is by using so called “atlas”, structures that combine the location and shape of anatomical structures and spatial relationships among them [9]. The main obstacle in “atlas” approaches is huge anatomical diversity. Recently, promising results in abdominal segmentation have been achieved using deep learning approaches [10-13], but these methods require large homogeny datasets. However, the greatest accuracy for abdominal organ segmentation has been obtained by multi-level hierarchical strategy combined with neural network approach [14], so in this paper we have used a hierarchical strategy for organ segmentation [15].

Dedicated clinical CT software usually presents independently stone scans, then the structure of the kidney itself, and finally the anatomy of the excretory system. These tools are not interactive, and they do not offer options for controlling the overall process of segmentation and 3D visualization. In this paper, we propose a flexible and interactive open-source tool, so called *3D Gastro CT tool*, for segmentation and 3D rendering of abdominal CT scans that could facilitate the urolithiasis treatment planning. In Section II we have presented the flowchart of the developed application, image preprocessing, segmentation and rendering methodology. Examples of the tool usage in patients with and without kidney stone are illustrated and compared with the output of the dedicated clinical software in Section III. Finally, the conclusion and plans for future work are given in Section IV.

II. The Method

3D Gastro CT tool was developed in Python language using the following libraries and toolkits: matplotlib [16], ndimage [17], SimpleITK (abstraction layer and wrapper around Insight Segmentation and Registration Toolkit, ITK) [18-20] and VTK (Visualization Toolkit) [21]. The graphical user interface (GUI) was developed using PyQt5 bindings for Qt v5 [22]. The code is available at Github link: https://github.com/milicevickatarina/3D-Gastro-CT.

Katarina Milićević is with the University of Belgrade - School of Electrical Engineering, Bulevar kralja Aleksandra 73, 11120 Belgrade, Serbia (e-mail: katarinamilicevic@gmail.com).

Otaš Durutović is with the School of Medicine, University of Belgrade, Department of Surgery and Anaesthesiology, Dr Subotića 8, Belgrade, Serbia and Clinical Centre of Serbia, Urology Clinic, Department of Urology, Resavska 51, Belgrade, Serbia (e-mail: odurutovic@gmail.com).

Milica Janković is with the University of Belgrade - School of Electrical Engineering, Bulevar kralja Aleksandra 73, 11120 Belgrade, Serbia (e-mail: piperski@etf.rs).

The flowchart of the developed application is shown in Fig. 1.

A. *Data management*

3D Gastro CT tool offers the option for reading and viewing a variety of 2D or 3D formats that are supported by SimpleITK reader (*Dicom*, *MetaImage* etc.). This allows the user to select the work directory with images and to explore available image files determining which files are appropriate for further processing.

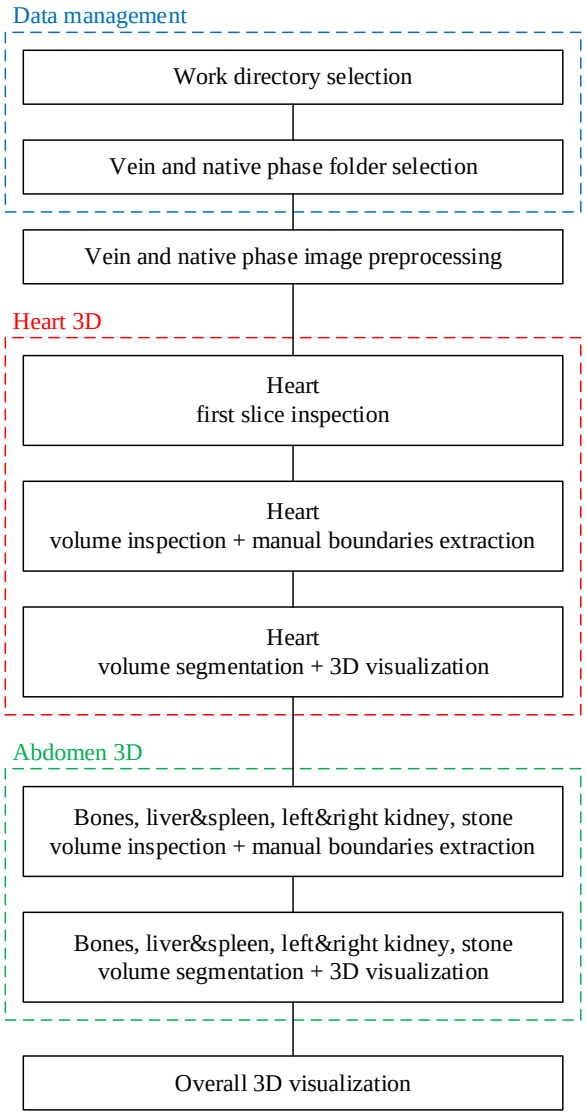

Fig. 1. Flowchart of the 3D Gastro CT tool

For the next step, "Image preprocessing", the selection of folders with native phase images (abdominal images recorded before CT contrast injection) and vein phase images (abdominal images recorded 70-80 s after the CT contrast injection) is necessary. The reason of using these two phases is that grey levels differ well: 1) in vein phase for heart, abdominal organs (liver, spleen, kidney) and stone 2) in native phase for skeleton (unlike vein phase where it overlaps with the intensity of the blood vessels).

Once performed, all preprocessing, segmentation and 3D rendering results would be stored for the future image retrieval. Export option in .stl and .jpg formats of individual and merged rendering results is available.

3D Gastro CT tool was tested using the dataset available from the routine CT imaging (Aquilion Prime CT Scanner, Toshiba Medical Systems, USA) performed for patients with suspected urinary tract stones in the Clinical Center of Serbia. The resolution of CT scans was 512x512 pixels and 588 CT slices in axial projection were available.

B. *Image preprocessing*

The images from the vein and native phases are preprocessed completely automatically using the following steps: 1) linear intensity transfer function for the band [-548, 800] to [0,255], 2) resampling images from 512x512 resolution to 256x256 to reduce time and space resources in further steps, 3) median filtering for noise reduction. Native phase was coregistered with the vein phase using the *SimpleITK* class *ImageRegistrationMethod* (similarity metric: mutual information (Mattes MI), interpolator: sitkLinear, optimizer: gradient descent), [23].

C. *3D segmentation*

The segmentation process is executed hierarchically, organ by organ, on the preprocessed images. The segmentation order is as follows: heart, bones, liver and spleen, kidneys and kidney stone. The segmentation of bones and kidney stone can be performed even if segmentation of previous organs is not finished. The result of individual organ segmentation is displayed rendered in the pop-up interactive window (rotation and zoom options enabled) so the user can decide to save or repeat the segmentation procedure.

C1. *Heart 3D segmentation*

Heart 3D segmentation performs on vein phases images. This procedure includes the following steps, Fig. 2:

- manual selection of heart rectangle region of interest (ROI) boundaries (left, right, upper, lower border) on the first CT slice, Fig. 2A
- fully automatic heart segmentation of the first CT slice using the following steps: 1) gaussian filtering (σ=2), Fig. 2B, 2) image binarization (threshold is set to 10 % of maximal pixel intensity), Fig. 2C, 3) the cross section between the heart rectangle ROI boundaries and the binary image, Fig. 2D, 4) filling holes and removing particles, Fig. 2E.
- fully automatic heart segmentation of the rest of CT slices containing heart using the following steps: 1) gaussian filtering (σ=2), 2) image binarization (threshold is set to 10 % of maximal pixel intensity), 3) the cross section of the binary image, heart rectangle ROI boundaries, and the dilated extracted heart ROI from the previous CT slice (dilation was used to compensate heart movements and different heart surface on successive CT slices)
- opening and closing of the extracted heart volume (cube structural element with the dimension 10).

C2. *Other organs' 3D segmentation*

Bones 3D segmentation performs on native phases images. The procedure is the same as in case of liver&spleen and

stone 3D segmentation. Liver&spleen and stone 3D segmentation performs on vein phases images. This procedure includes the following steps:

- histogram presentation for the whole CT volume
- manual selection of upper and lower threshold that correspond to the VOI intensity boundaries on the histogram for image binarization as it is defined in Fig. 3A, B, C (left)
- volume binarization performs on the volume where the heart and bones VOIs are removed for liver&spleen segmentation
- opening and closing of the extracted volume (cube structural element with the dimension 3).

Kidney 3D segmentation performs on vein phases images. This procedure includes the following steps, Fig. 3D:

- manual selection of kidney VOI boundaries (top and bottom slice number, left, right, upper, lower border) that cover the kidney VOI in all CT slices
- histogram presentation for the kidney VOI where bones and liver&spleen volumes are previously removed
- manual selection of upper and lower threshold that correspond to the kidney intensity boundaries on the histogram for volume binarization as it is defined in Fig. 3D (left)
- the cross section between the kidney VOI boundaries and the binary image
- opening and closing of the extracted kidney volume (cube structural element with the dimension 4).

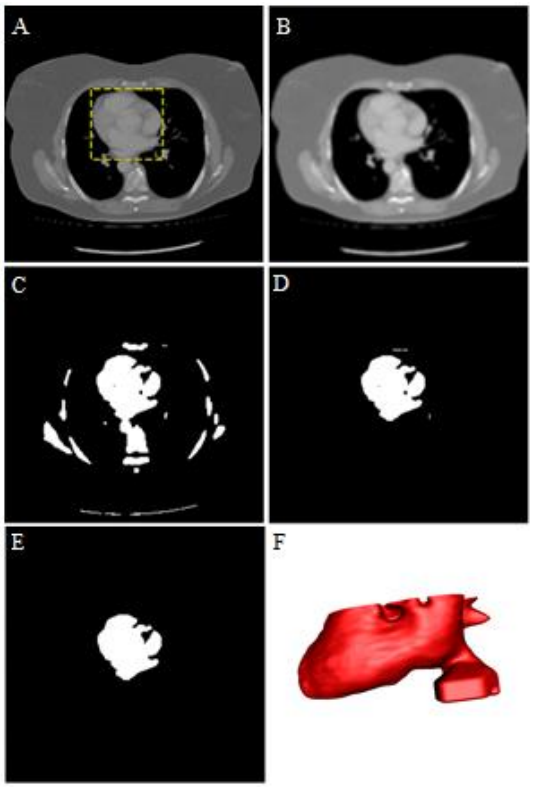

Fig. 2. Heart 3D segmentation process: A) manual selection of heart rectangle ROI boundaries, B) gaussian filtering, C) image binarization, D) cross section with rectangle ROI, E) filling holes and removing particles, F) 3D heart rendering result

D. 3D visualization

3D rendering was performed using the *Marching Cubes* algorithm [24] using the implementation presented in [25]. Segmented images are archived in *.mhd* format compatible with the VTK reader. Individual segmentation results are merged to perform the overall 3D visualization.

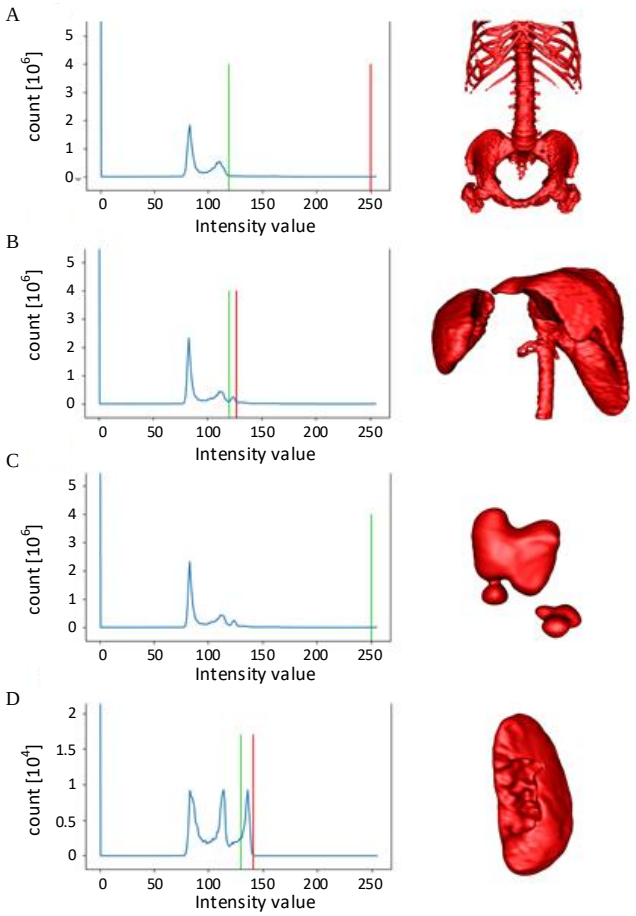

Fig. 3. Bones (A), liver&spleen (B), stone (C), and kidney (D) upper and lower threshold selection on corresponding histograms (left) and individual 3D rendering results (right)

III. RESULTS

An example of the GUI for semi-automated left and right kidney segmentation is shown in Fig. 4. Numerical controls are used for setting values of VOI boundaries. Histogram display is used for determination of lower and upper thresholds. Pop-up windows are used for checking selected kidney boundaries and the display of individual kidney 3D rendering results.

Fig. 5 presents the comparison of the 3D visualization results from *3D Gastro CT tool* and dedicated clinical software for two subjects: the first one is without kidney stone and the second one is with the left kidney stone. For the second subject, the displays are without showing liver and spleen volumes. It could be observed that *3D Gastro CT tool* offers more selectivity in the display where disturbing blood vessels can be completely removed.

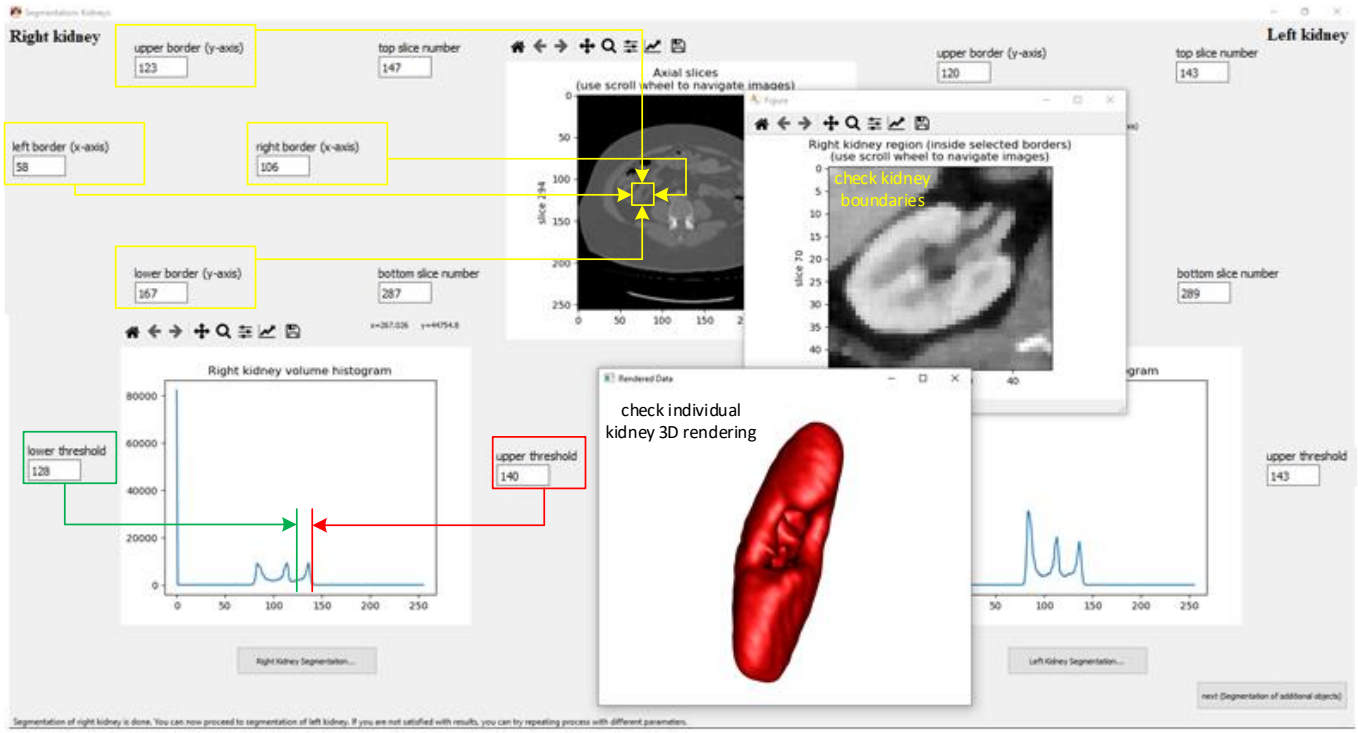

Fig. 4. An example of GUI for setting boundaries and thresholds for the left and right kidney segmentation process, checking boundaries and individual kidney 3D rendering

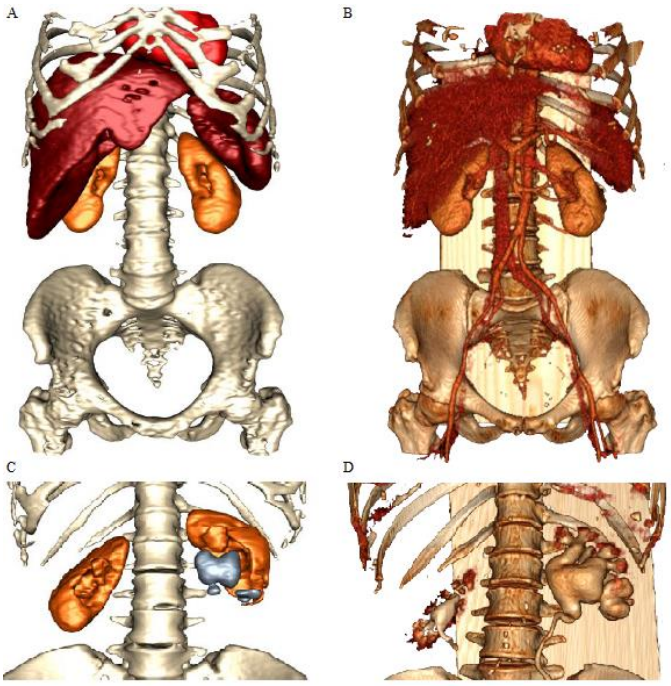

Fig. 5. The comparison of the 3D visualization results from *3D Gastro CT tool* (left) and dedicated clinical software (right) for the patient without (up) and with (down) kidney stone

IV. Conclusion

An open-source semi-automated solution for the visualization of abdomen in patients with urolithiasis is presented in the paper. The segmentation process of individual organs is sequential, and necessary inputs for the realized *3D Gastro CT tool* are native and vein phase CT slices of abdomen. The advantages of the developed tool are demonstrated through examples that are compared with the output from the dedicated clinical software. The usage of the tool is presented on the specific type of urologic CT study, but it is flexible to expand to a wider range of applications. Future work will be focused on testing of the tool on a larger clinical dataset and improving it by the completely automatic algorithm for segmentation.

Acknowledgment

This research was supported by the Ministry for Education, Science and Technology Development of Serbia, Belgrade, Serbia. The authors are especially grateful to dr Milica Stojadinović on the interpretation of CT scans.

References

[1] E. P. Balogh, B. T. Miller, J. R. Ball, *Improving diagnosis in health care*, Washington, USA: National Academies Press, 2015.

[2] J. M. Weinrich, P. Bannas, M. Regier, S. Keller, L. Kluth, G. Adam, F. O. Henes, „Low-dose CT for evaluation of suspected urolithiasis: diagnostic yield for assessment of alternative diagnoses", *American Journal of Roentgenology*, vol. *210*, no. *3*, pp. *557-563*, 2018.

[3] L. Tzelves, C. Türk, A. Skolarikos, „European Association of Urology Urolithiasis Guidelines: Where Are We Going?", *European Urology Focus*, vol. *7*, no. *1*, pp. *34–38*, 2021.

[4] C. Türk, A. Neisius, A. Petrik, A. Seitz, A. Skolarikos, K. Thomas K, G. Gambaro, „Urolithiasis", European Association of Urology Guidelines, Available from: https://uroweb.org/guideline/urolithiasis/ (last access June 2021)

[5] D. Assimos, A. Krambeck, N. L. Miller, M. Monga, M. H. Murad, C. P. Nelson, K.T. Pace, V. M. Pais, M. S. Pearle, G. M. Preminger, H. Razvi, O. Shah, B. R. Matlaga, „Surgical Management of Stones: AUA/Endourology Society Guideline", Available from: https://www.auanet.org/guidelines/kidney-stones-surgical-management-guideline#x3158 (last access June 2021)

[6] B. Baralo, P. Samson, D. Hoenig, A. Smith, „Percutaneous kidney stone surgery and radiation exposure: A review", *Asian journal of urology*, vol. *7*, no. *1*, pp. *10–17*, 2020.
[7] O. Durutović, „Evaluation of percutaneous nephrolithotomy efficasy in the treatment of patients with kidney stone", PhD thesis, University of Belgrade, School of Medicine, Belgrade, Serbia, 2016.
[8] A. C. Westphalen, R. Y. Hsia, J. H. Maselli, R. Wang, R. Gonzales, „Radiological imaging of patients with suspected urinary tract stones: national trends, diagnoses, and predictors", *Academic emergency medicine : official journal of the Society for Academic Emergency Medicine*, vol. *18*, no. *7*, pp. *699–707*, 2011.
[9] B. Oliveira, S. Queirós, P. Morais, H. R. Torres, J. Gomes-Fonseca, J. C. Fonseca, J. L. Vilaça. „A novel multi-atlas strategy with dense deformation field reconstruction for abdominal and thoracic multi-organ segmentation from computed tomography", *Medical Image Analysis*, vol. *45*, pp. *108-120*, 2018.
[10] O. Ronneberger, P. Fischer, T. Brox T, „U-Net: Convolutional Networks for Biomedical Image Segmentation", In: Navab N., Hornegger J., Wells W., Frangi A. (eds) Medical Image Computing and Computer-Assisted Intervention - MICCAI 2015. MICCAI 2015. Lecture Notes in Computer Science, vol. *9351*, pp. *234-241*, Springer, Cham, 2015.
[11] F. Milletari, N. Navab, S. A. Ahmadi, „V-Net: Fully Convolutional Neural Networks for Volumetric Medical Image Segmentation", Fourth International Conference on 3D Vision (3DV), pp. *565-571*, Stanford, CA, 2016.
[12] P. Hu, F. Wu, J. Peng, Y. Bao, F. Chen, D. Kong, „Automatic abdominal multi-organ segmentation using deep convolutional neural network and time-implicit level sets", *International Journal of Computer Assisted Radiology and Surgery*, vol. *12*, no. *3*, pp. *399–411*, 2017.
[13] E. Gibson, F. Giganti, Y. Hu, E. Bonmati, S. Bandula, K. Gurusamy, B. Davidson, S. P. Pereira, M. J. Klarkson, D. C. Barratt, „Automatic Multi-Organ Segmentation on Abdominal CT With Dense V-Networks", *IEEE Transactions on Medical Imaging*, vol. *37*, no. *8*, pp. *1822-1834*, 2018.
[14] M. A. Selver, „Segmentation of abdominal organs from CT using a multi-level, hierarchical neural network strategy", *Computer Methods and Programs in Biomedicine*, vol. *113*, no. *3*, pp. *830-852*, 2014.
[15] K. Milićević, „3D segmentation and visualization of abdominal computed tomography scans", BSc. Thesis, University of Belgrade – School of Electrical Engineering, Belgrade, Serbia, 2020.
[16] J. D. Hunter, „Matplotlib: A 2D Graphics Environment", *Computing in Science & Engineering*, vol. *9*, no. *3*, pp. *90-95*, 2007.
[17] https://docs.scipy.org/doc/scipy/reference/ndimage.html (last access June 2021)
[18] W. Schroeder, K. Martin, B. Lorensen, *The Visualization Toolkit*, 4th ed, New York, USA: Kitware, 2006.
[19] R. Beare, B. C. Lowekamp, Z. Yaniv, „Image Segmentation, Registration and Characterization in R with SimpleITK", *J Stat Softw*, vol. *86*, no. *8*, pp. *6595*, 2018.
[20] Z. Yaniv, B. C. Lowekamp, H. J. Johnson, R. Beare, „SimpleITK Image-Analysis Notebooks: a Collaborative Environment for Education and Reproducible Research", *J Digit Imaging*, vol. *31*, no. *3*, pp. *290-303*, 2018.
[21] B. C. Lowekamp, D. T. Chen, L. Ibáñez, D. Blezek, „The Design of SimpleITK", *Front. Neuroinform*, vol. *7*, no. *45*, pp. 1-14, 2013.
[22] https://pypi.org/project/PyQt5/ (last access June 2021)
[23] https://github.com/InsightSoftwareConsortium/SimpleITK-Notebooks/blob/master/Python/60_Registration_Introduction.ipynb (last access June 2021)
[24] W. E. Lorensen, H. E. Cline, „Marching cubes: A high resolution 3D surface construction algorithm", *ACM siggraph computer graphics*, vol. *21*, no. *4*, pp. *163-169*, 1987.
[25] https://github.com/lorensen/VTKExamples (last access June 2021)